AD-A032 698 BALLISTIC RESEARCH LABS ABERDEEN PROVING GROUND MD F/G 4/1
SYNOPSIS OF IONIZATION SOURCES IN THE MESOSPHERE AND STRATOSPHE--ETC(U)
OCT 76 M G HEAPS

UNCLASSIFIED BRL-1938 NL

| OF |
AD
A032698

END

DATE
FILMED
1-77

BRL

REPORT NO. 1938

SYNOPSIS OF IONIZATION SOURCES IN THE MESOSPHERE AND STRATOSPHERE, WITH PARTICULAR EMPHASIS GIVEN TO THE PATH OF THE 26 FEBRUARY 1979 SOLAR ECLIPSE

Melvin G. Heaps

October 1976

USA BALLISTIC RESEARCH LABORATORIES
ABERDEEN PROVING GROUND, MARYLAND

Destroy this report when it is no longer needed.
Do not return it to the originator.

Secondary distribution of this report by originating or sponsoring activity is prohibited.

Additional copies of this report may be obtained from the National Technical Information Service, U.S. Department of Commerce, Springfield, Virginia 22151.

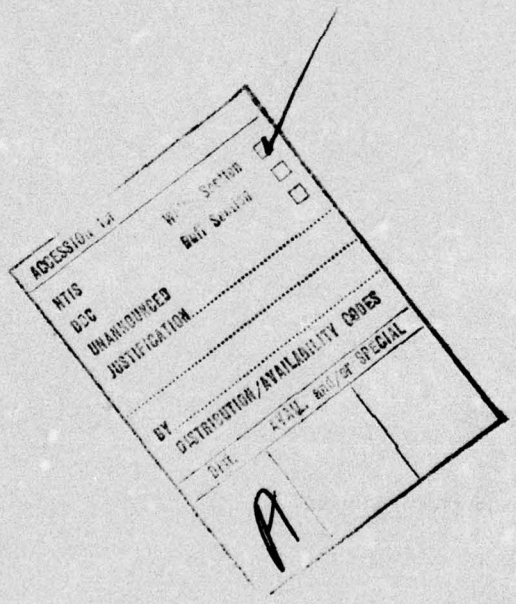

The findings in this report are not to be construed as an official Department of the Army position, unless so designated by other authorized documents.

UNCLASSIFIED

SECURITY CLASSIFICATION OF THIS PAGE *(When Data Entered)*

REPORT DOCUMENTATION PAGE

READ INSTRUCTIONS BEFORE COMPLETING FORM

1. REPORT NUMBER: BRL REPORT NO. 1938
2. GOVT ACCESSION NO.
3. RECIPIENT'S CATALOG NUMBER
4. TITLE *(and Subtitle)*: SYNOPSIS OF IONIZATION SOURCES IN THE MESOSPHERE AND STRATOSPHERE, WITH PARTICULAR EMPHASIS GIVEN TO THE PATH OF THE 26 FEBRUARY 1979 SOLAR ECLIPSE
5. TYPE OF REPORT & PERIOD COVERED: Final rept.
6. PERFORMING ORG. REPORT NUMBER
7. AUTHOR(s): Melvin G. Heaps (NRC/BRL Research Associate)
8. CONTRACT OR GRANT NUMBER(s)
9. PERFORMING ORGANIZATION NAME AND ADDRESS: US Army Ballistic Research Laboratory, Aberdeen Proving Ground, MD 21005
10. PROGRAM ELEMENT, PROJECT, TASK AREA & WORK UNIT NUMBERS: RDT&E 1T162111AH71
11. CONTROLLING OFFICE NAME AND ADDRESS: US Army Materiel Development & Readiness Command, 5001 Eisenhower Avenue, Alexandria, VA 22333
12. REPORT DATE: OCTOBER 1976
13. NUMBER OF PAGES: 45
14. MONITORING AGENCY NAME & ADDRESS *(if different from Controlling Office)*: 41p.
15. SECURITY CLASS. *(of this report)*: Unclassified
15a. DECLASSIFICATION/DOWNGRADING SCHEDULE

16. DISTRIBUTION STATEMENT *(of this Report)*

Approved for public release; distribution unlimited.

17. DISTRIBUTION STATEMENT *(of the abstract entered in Block 20, if different from Report)*

18. SUPPLEMENTARY NOTES

19. KEY WORDS *(Continue on reverse side if necessary and identify by block number)*

Ion-pair production rate
Ionization
Stratosphere
Mesosphere

20. ABSTRACT *(Continue on reverse side if necessary and identify by block number)* (KST)

The sources of ionization in the mesosphere and stratosphere may be placed in three categories: solar radiation (photons), galactic cosmic rays, and precipitating energetic particles of solar and terrestrial origin and modulation. The ion-pair production rate Q (ion pairs per cubic centimeter per second) due to x-rays and EUV radiation is a function of latitude, time of day, solar declination, and the solar sunspot cycle. Solar radiation dominates the Q term in the upper mesosphere during the day. Galactic cosmic rays are the major

(Continued on reverse side)

DD FORM 1 JAN 73 1473 EDITION OF 1 NOV 65 IS OBSOLETE

UNCLASSIFIED 050 250

SECURITY CLASSIFICATION OF THIS PAGE *(When Data Entered)*

LB

20. ABSTRACT (Continued)

source of ion pairs at night throughout the stratosphere and lower mesosphere and even into the upper mesosphere during geomagnetically quiet conditions. The Q term due to galactic cosmic rays also displays a dependence on latitude and the solar cycle. Energetic particles (electrons > 40 keV, protons > 1 MeV, alpha particles > 5 MeV) can be the dominant source of ion pairs for short times in the stratosphere and mesosphere, competing with even solar radiation under some circumstances. The effects are more prominent at higher latitudes, particularly for protons.

Special attention is given to the probable ionization sources along the path of the 26 February 1979 solar eclipse and particularly to the various zones of precipitating particles as this path crosses the North American continent.

TABLE OF CONTENTS

LIST OF ILLUSTRATIONS

LIST OF ILLUSTRATIONS (CONT.)

I. INTRODUCTION

The mesosphere and stratosphere, those sections of the earth's atmosphere ranging from approximately 85 km down to as low as 10 km, are ionized by both particles and photons. It is convenient to place the sources of ionization into three broad categories: solar radiation in the x-ray and extreme ultraviolet wavelengths, galactic cosmic rays and other galactic radiations, and precipitating energetic particles of solar origin and terrestrial modulation. Minor sources such as bremsstrahlung, lightning and naturally occurring radioactivity will not be considered here.

Direct solar radiation is the largest source of ions in the upper atmosphere, forming the E and F regions of the ionosphere and also the D region which encompasses the upper mesosphere. There is obviously a large day-night fluctuation, with latitude, season and solar cycle also being important factors. Galactic cosmic rays are generally the largest source of ions in the stratosphere and lower mesosphere. There are (essentially) no diurnal or seasonal variations, but changes in latitude and the solar sunspot cycle are important. Galactic x-rays are a minor source of ionization in the mesosphere, usually masked by other sources. Particle precipitation is an extremely variable yet important source of ionization in the mesosphere and occasionally the stratosphere. Protons of more than 1 MeV energy are capable of penetrating into the mesosphere but are usually a very minor source at lower latitudes. Over the polar caps, however, and extending to latitudes as low as 60°, protons can cause large amounts of ionization even in the stratosphere. Electrons of more than 40 keV can also penetrate below the mesopause. Fluxes of such electrons increase with increasing latitude, and large quantities may also be present when protons are precipitating. While it is understood that all of the above sources ionize higher regions of the atmosphere, the emphasis of this paper will be on the mesosphere and stratosphere.

II. SOLAR RADIATION

Direct ionization by solar photon radiation occurs within the mesosphere and can be attributed to x-rays, which ionize all atmospheric constituents, and that portion of the EUV radiation > 100 nm, which is capable of ionizing several minor constituents, particularly nitric oxide (NO).

The x-ray flux may be divided into two components - hard x-rays (< 1 nm) and soft x-rays (3.1-10 nm). The flux in the intermediate range of 1-3.1 nm is smaller than the soft x-ray flux but is absorbed over the same altitude range and is generally neglected with respect to the soft x-ray flux.

The variation of x-ray fluxes with the solar cycle is large, particularly for the hard x-rays where a fluctuation of 100 X is not uncommon. Figure 1 illustrates some representative fluxes for the entire range of 0.1-10 nm (patterned mainly after Swider;[1] see also Banks and Kockarts,[2] and Nicolet and Aikin[3]). The fluxes shown are representative averages for quiet solar sunspot conditions during a solar cycle minimum and for quiet and lightly disturbed sunspot conditions during a solar cycle maximum. The variation in the soft x-ray flux is generally contained within an order of magnitude. Solar flares may cause the hard x-ray flux to increase up to two orders of magnitude over the values shown, with a corresponding increase of about 3 X in the soft x-ray flux. Table I contains the representative penetration depths for various wavelengths.

Figure 2 shows the spread in ion-pair production rates due to various x-ray fluxes. The soft x-rays do not appreciably affect the ionization within the mesosphere and will henceforth be neglected. Other wavelengths between 10 nm and 100 nm are absorbed in the thermosphere and do not penetrate to mesospheric heights.

Solar EUV radiation in the range of 100-130 nm does penetrate to the mesosphere and is capable of ionizing O_2 and several minor constituents. Of particular importance are the Lyman β line at 102.6 nm, able to ionize O_2, and the Lyman α line at 121.6 nm, able to ionize NO. The concentration of NO, denoted by [NO] in molecules cm^{-3}, is a critical factor in determining the ion-pair production rate profile. Two ranges of possible NO concentrations are shown in Figure 3. In addition to the question of the order of magnitude of [NO], the question of whether the minimum occurs near 70 km or above 80 km is critical. Figure 4 shows the ion-pair production rate for the two ranges of [NO]. Fluctuations in the flux of Lyman α are not as critical at this point as the uncertainties in [NO] near 70 km. Also shown for comparison are the median values for hard x-rays. In all subsequent figures where the NO^+ ionization profile is used, the NO density of Meira[4] has been employed.

---

[1] Swider, W., Jr., Ionization rates due to the attenuation of 1-100Å nonflare solar x-rays in the terrestrial atmosphere, Rev. Geophysics, 7, 573-594, 1969.

[2] Banks, P.M. and G. Kockarts, Aeronomy, Part A, Academic Press, New York, 1973.

[3] Nicolet, M. and A.C. Aikin, The formation of the D region of the ionsphere, J. Geophys. Res., 65, 1469-1483, 1960.

[4] Meira, L.G., Rocket measurements of upper atmospheric nitric oxide and their consequences to the lower ionsphere, J. Geophys. Res., 76, 202-212, 1971.

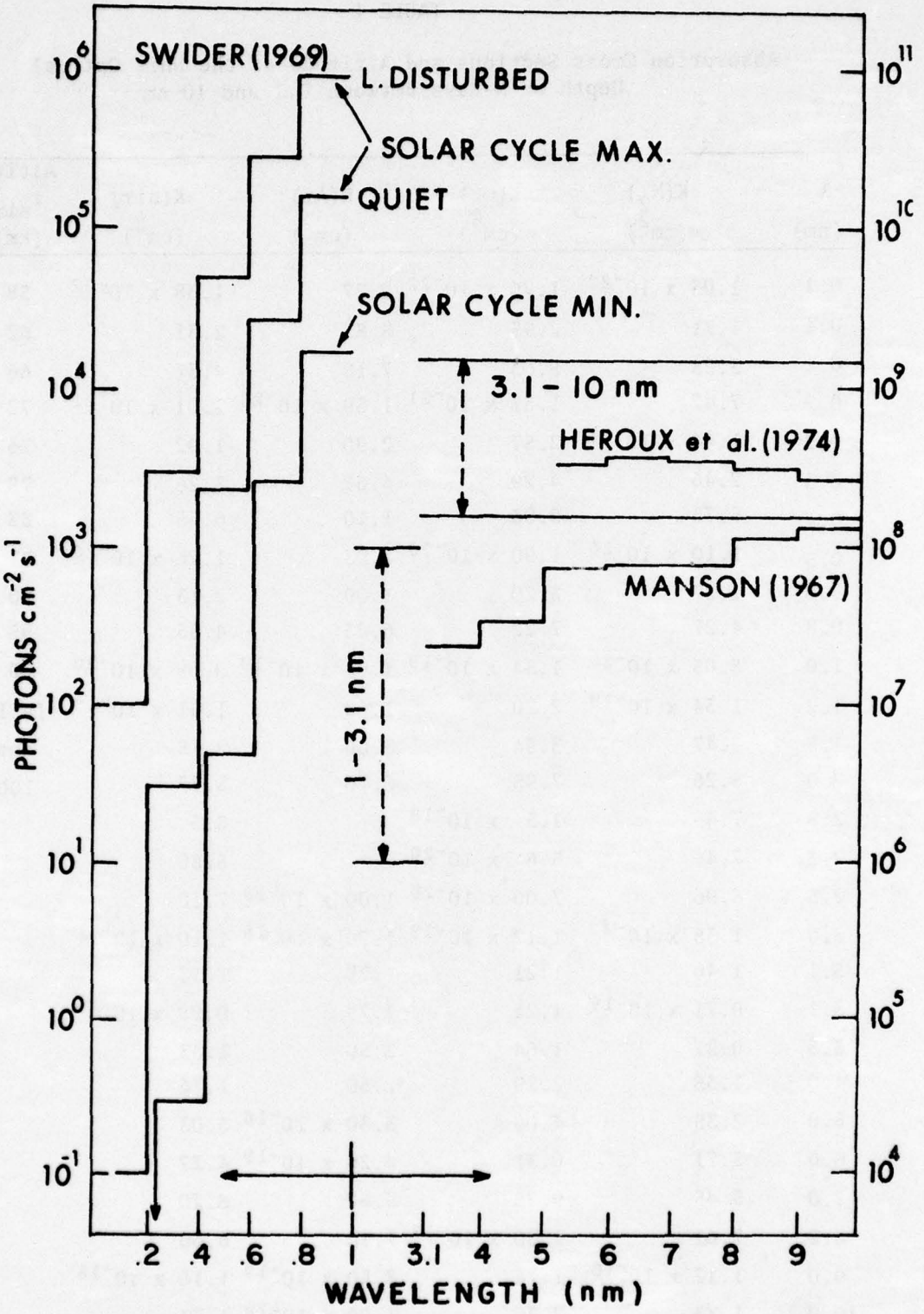

Figure 1. The variations in the solar x-ray flux. Note the different scales for hard and soft x-rays. The horizontal lines bracketing the dashed arrows give the range of the integrated flux over the appropriate wavelength regions.

TABLE I

Absorption Cross Sections and Altitude of the Unit Optical Depth of X-Rays Between 0.1 and 10 nm

λ (nm)	$K(N_2)$ (cm^2)	$K(O_2)$ (cm^2)	K(Ar) (cm^2)	K(air) (cm^2)	Altitude $\tau_{air}=1$ (km)
0.1	1.03×10^{-22}	1.76×10^{-22}	2.27	1.38×10^{-22}	58
0.1	1.71	2.95	3.83	2.31	62
0.1	3.23	5.63	7.18	4.37	66
0.2	7.47	1.31×10^{-21}	1.59×10^{-20}	1.01×10^{-21}	72
0.2	1.44×10^{-21}	2.57	2.90	1.92	76
0.3	2.46	4.29	4.67	3.26	79
0.4	5.73	9.93	1.10	6.55	83
0.5	1.10×10^{-20}	1.90×10^{-20}	1.93	1.26×10^{-20}	87
0.6	1.87	3.20	3.09	2.13	90
0.8	4.27	7.22	6.23	4.85	95
1.0	8.05×10^{-20}	1.34×10^{-19}	1.05×10^{-19}	9.09×10^{-20}	99
1.2	1.34×10^{-19}	2.20	1.60	1.51×10^{-19}	(all
1.5	2.47	3.94	3.00	2.75	above
2.0	5.26	7.95	6.16	5.77	100 km)
2.3	7.4	1.3×10^{-18}		8.5	
2.3	7.4	5.6×10^{-20}		5.80	
2.5	8.96	7.00×10^{-20}	1.00×10^{-18}	7.10	
3.0	1.38×10^{-18}	1.12×10^{-19}	1.70×10^{-18}	1.10×10^{-18}	
3.1	1.40	1.21	1.79	1.15	
3.1	0.71×10^{-19}	1.21	1.79	0.98×10^{-19}	
3.5	0.97	1.64	2.50	1.33	
4.0	1.35	2.29	2.50	1.76	
5.0	2.35	4.00	3.80×10^{-18}	3.03	
6.0	3.71	6.31	4.20×10^{-19}	4.22	
7.0	5.45	9.28	5.60	6.20	
8.0	7.61	1.30×10^{-18}	7.10	8.66	
9.0	1.12×10^{-18}	1.74	8.50×10^{-19}	1.16×10^{-18}	
10.0	1.33	2.26	1.00×10^{-18}	1.57	

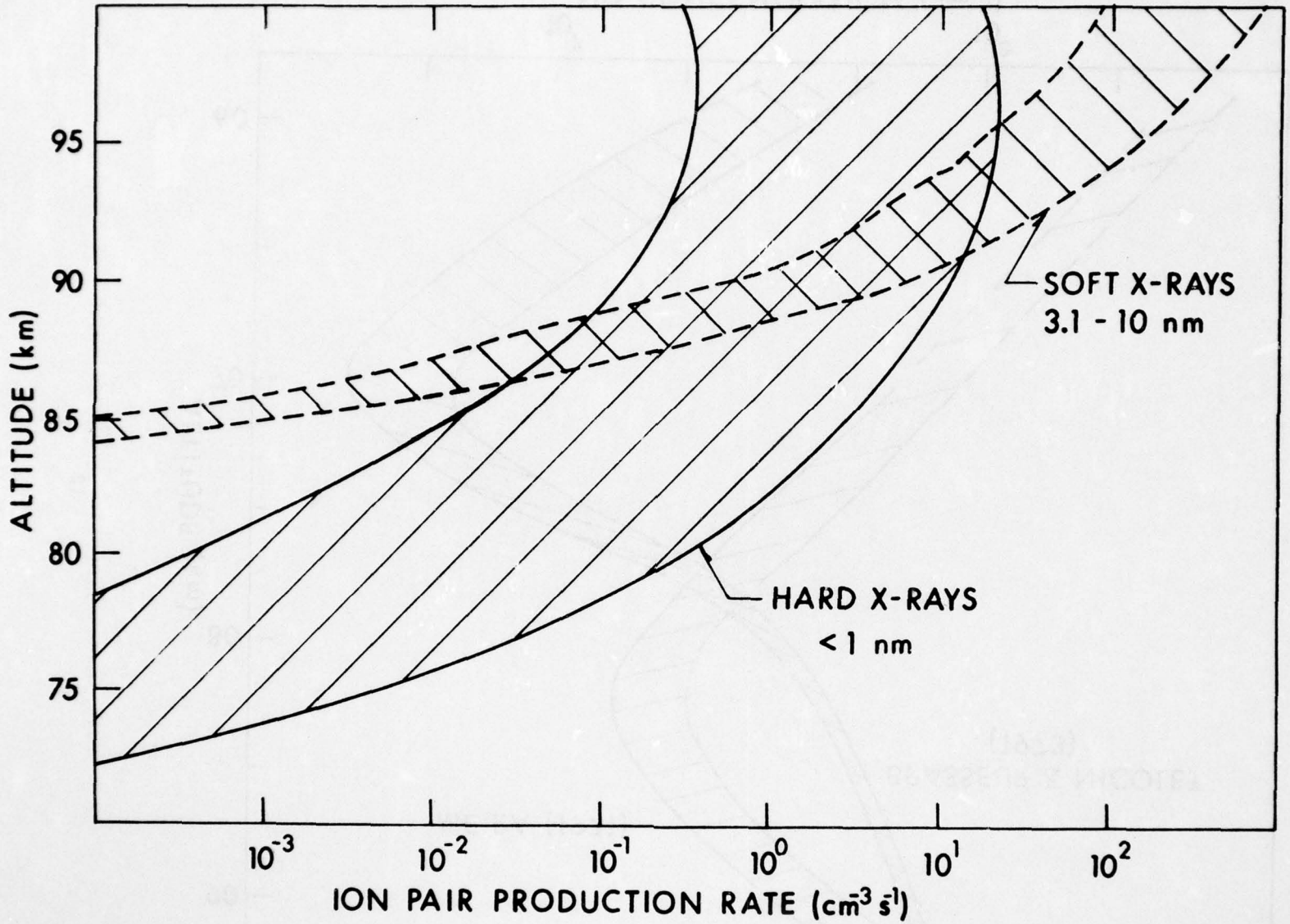

Figure 2. The range of ion-pair production rates due to fluctuations in the solar x-ray flux.

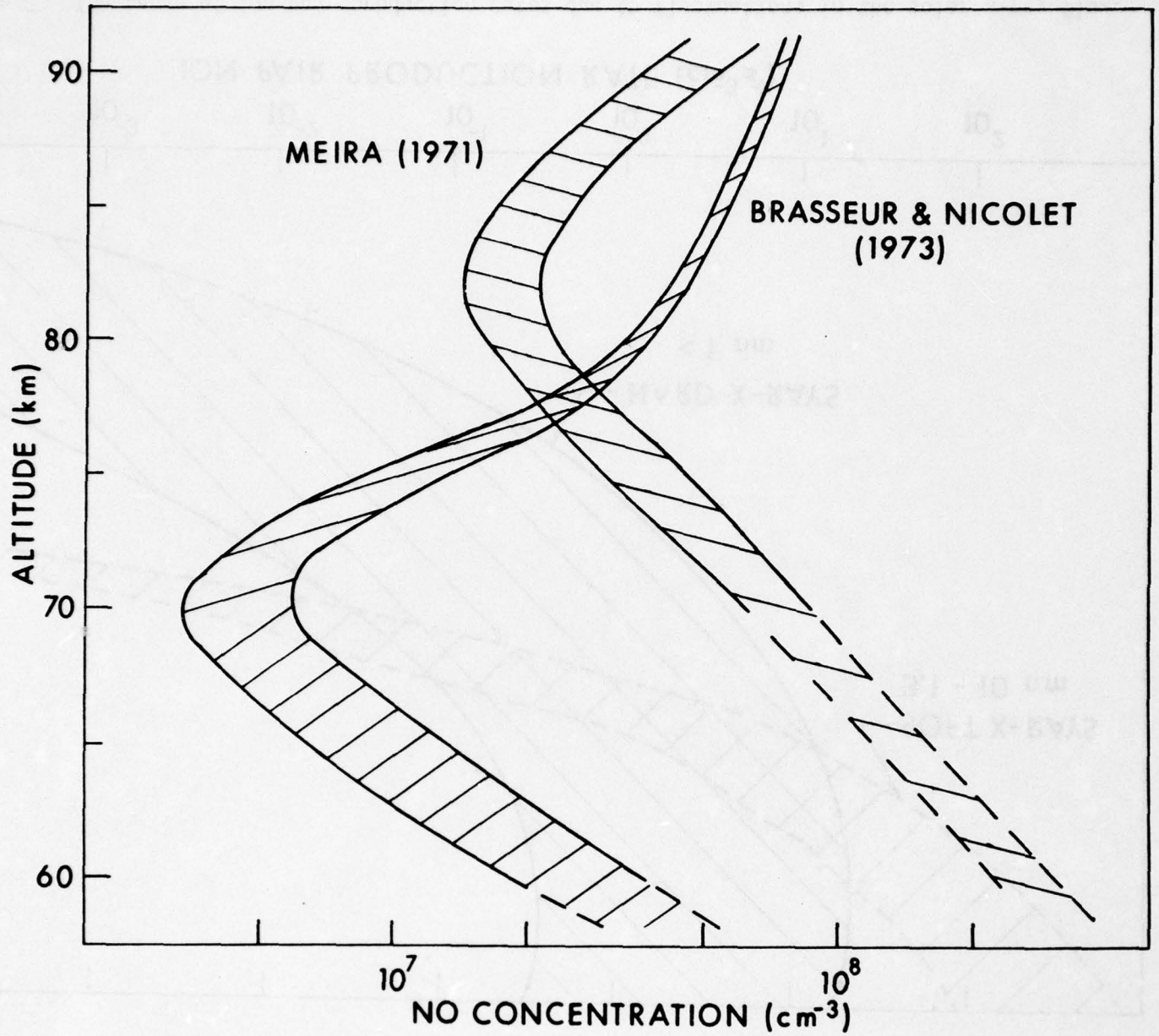

Figure 3. The uncertainties in the nitric oxide density profile.

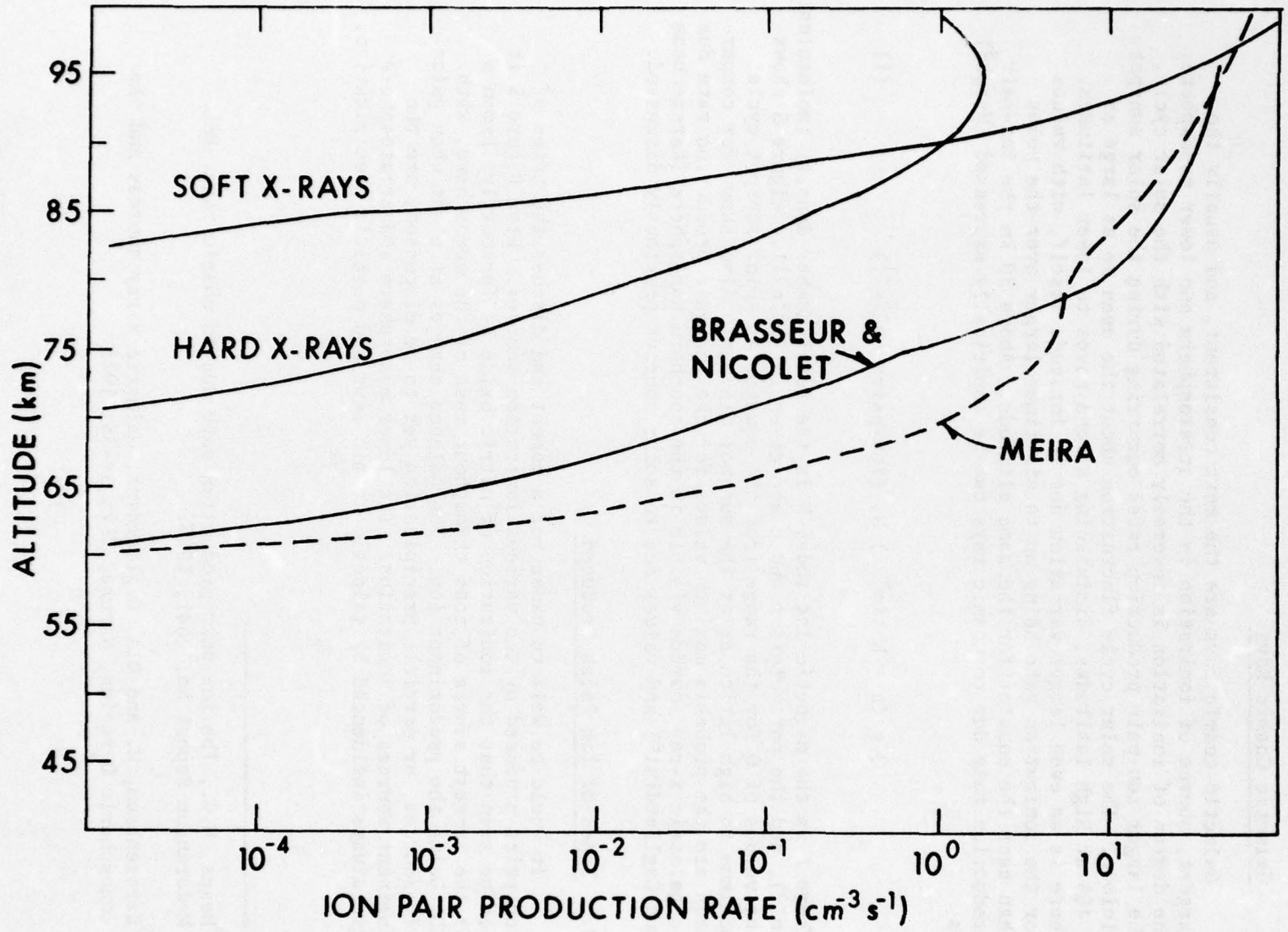

Figure 4. The NO^+ production rate for the two [NO] profiles from Figure 3. Also shown are representative ion-pair production rates for x-rays shown in Figure 2.

A. Galactic Cosmic Rays

Galactic cosmic rays are the most consistent, and usually the largest, source of ionization in the stratosphere and lower mesosphere. The degree of ionization is inversely correlated with the solar cycle, the larger ion-pair production rates occurring during the solar sunspot minimum. The solar cycle fluctuation about the mean is as large as ± 40% at high latitudes, diminishing as one moves to lower latitudes. There is an even larger variation due to latitude itself, with values for the ionization rate being up to six times larger over the poles than near the equator for the same altitude. Above 30 km the ion-pair production rate due to cosmic rays can be empirically expressed (Heaps[5]) as

$$Q = (a + b \sin^4 \Lambda)\, N, \text{ (ion-pairs cm}^{-3}\text{s}^{-1}\text{)} \qquad (1)$$

where Λ is the magnetic latitude, N is the total number density (molecules cm^{-3}), and the parameters a and b are given in Table II. Figure 5 shows the values of Q for the range from the equator at solar sunspot cycle maximum to high latitudes at the sunspot minimum. Also shown for comparison are the probable maximum values for the ion-pair production rate due to galactic x-ray sources visible in the southern hemisphere (Karszenbaum and Gagliardini[6]) and values due to solar sources previously discussed.

B. Types of Ion Pairs Produced

It would be well to pause for a moment and discuss the types of ion-pairs produced by the various ionization sources. From Figure 5 it can be seen that the ionization of nitric oxide by (primarily) Lyman α is the largest source of ions throughout most of the mesosphere, with NO^+ being the predominant ion. The balance changes at night when galactic sources, or particle precipitation yet to be discussed, are the dominant sources of ionization. The lower mesosphere and stratosphere are always influenced by galactic cosmic rays and particle precipitation.

---

[5]Heaps, M.G., The ion-pair production rate due to cosmic rays. BRL Memorandum Report No. 2641, 1976.

[6]Karszenbaum, H. and D.A. Gagliardini, Galactic x-ray sources and the ionospheric D region, Nature, 257, 34-35, 1975.

TABLE II

	High Altitude Range above 30 km	
	a	b
Q_{max} (1965 solar min.)	1.63×10^{-18}	31.4×10^{-18}
Q_{min} (1958 solar max.	1.63×10^{-18}	18.8×10^{-18}

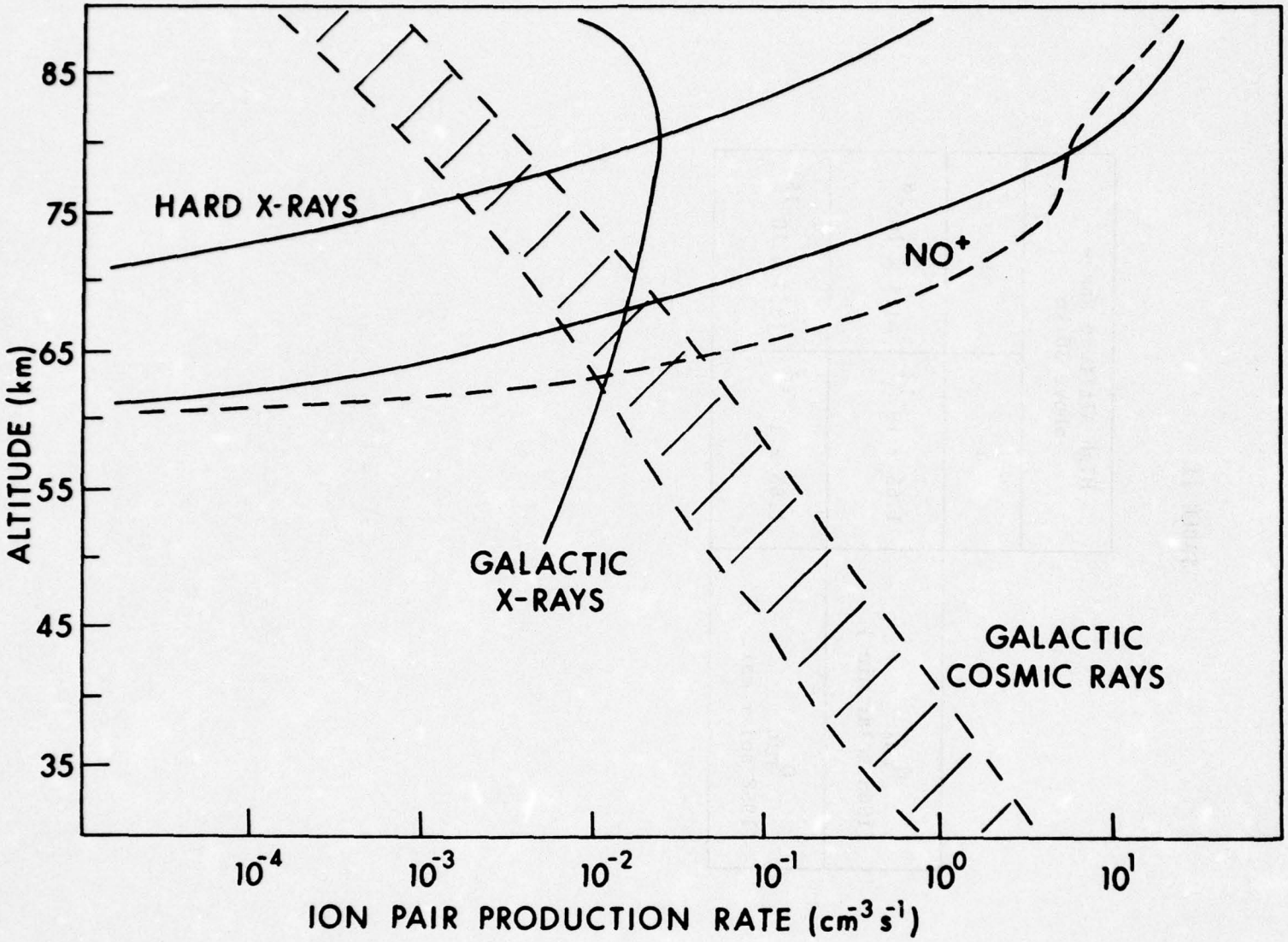

Figure 5. The ion-pair production rates for galactic cosmic rays. Also shown for comparison are maximum rates for galactic x-rays (southern hemisphere) and representative solar sources.

Hard solar x-rays ionize N_2 and O_2 principally by ejecting a K-shell electron. The molecule readjusts through an Auger process, ejecting yet another electron. For example

$$N_2 + h\nu \rightarrow N_2^+ + e \xrightarrow[\text{Process}]{\text{Auger}} N_2^{++} + 2e \,. \qquad (2)$$

The doubly-ionized molecule quickly undergoes dissociative charge exchange with another molecule, so that

$$N_2^{++} + N_2 \rightarrow N_2^+ + N^+ + N \,. \qquad (3)$$

An analogous process occurs with molecular oxygen. However, it is the primary photoelectron, with several hundred eV to several keV energy, and the Auger electron, with several hundred eV energy, that provide most of the resultant ionization. Dissociative ionization is an appreciable part of the total ionization (Rapp, et al.[7]) and produces significant amounts of the atomic ions and atoms, particularly important with respect to nitrogen.

$$N_2 + e \rightarrow N_2^+ + 2e \qquad (80\%) \qquad (4a)$$

$$\rightarrow N^+ + N + 2e \qquad (20\%) \qquad (4b)$$

$$O_2 + e \rightarrow O_2^+ + 2e \qquad (70\%) \qquad (4c)$$

$$\rightarrow O^+ + O + 2e \qquad (30\%) \qquad (4d)$$

Upwards of 95% of the total ionization due to x-rays is from the secondary electrons. The subsequent dissociation of N_2 by electrons (Winters[8]) is a significant source of neutral atomic nitrogen, with important consequences in the NO budget.

---

[7] Rapp, D., P. Englander-Golden and D.D. Briglia, Cross sections for dissociative ionization of molecules by electron impact, J. Chem. Phys., 42, 4081-4086, 1965.

[8] Winters, H.F., Ionic absorption and dissociation cross section for nitrogen, J. Chem. Phys., 44, 4472-4476, 1966.

The ionization by galactic cosmic rays and particle precipitation also proceeds mainly through secondary electrons, with the products the same as in equations 4a - d. During solar particle events, when the particle ionization may even exceed the daytime solar source, the structure of the ion chemistry is significantly altered.

C. Particle Precipitation

The objective here will be to provide a brief overview of the magnitude and types of particle fluxes as a function of latitude. Where it is possible, estimates of the fluctuations, time and longitudinal variations will also be given. Because interest lies in ionization in the stratosphere and mesosphere, only electrons of > 40 keV energy and protons of > 1 MeV energy will be considered. Alpha particles of more than 5 MeV energy may also penetrate into the mesosphere, but their effect is estimated to be only a few percent that of precipitating protons and will henceforth be neglected.

D. Electron Precipitation

The measurements of both precipitating and trapped energetic particles are most often carried out by satellite-borne detectors. Thus while the broad patterns of electron precipitation as a function of latitude are obtained, more specific information as to the variation with longitude and local time is generally unavailable. Figure 6 represents the average fluxes from several different measurements and roughly illustrates the dependence on magnetic latitude. The flux is given as the total number of particles above a certain threshold (the 40 keV lower limit of a Geiger counter) per unit area, per unit time, per unit solid angle. Isotropic angular distribution over the loss cone is usually assumed. The data is most easily arranged in patterns when the magnetic latitude Λ and the L-shell parameter are used. At the point where a given L-shell intersects the earth one has to a first approximation $L \cos^2 \Lambda = 1$.

The trapped radiation belts are generally given a lower boundary of between L = 1.1 and 1.2. This means that the lowest latitudes, say below $\Lambda = 25°$, have a very low particle precipitation rate. Actual measurements are sparse, and therefore a reasonable estimate for the electron precipitation is $j\ (E > 40\ \text{keV}) \leq 10^2$ electrons $cm^{-2}\ sec^{-1}\ sr^{-1}$. As one moves from the low to the middle latitude range, from $\Lambda = 25° - 40°$, the flux of precipitating electrons increases and may reach up to 10^3 electrons $cm^{-2}\ sec^{-1}\ sr^{-1}$, but again the number of measurements is small.

Because the earth's magnetic and geographic axes do not coincide, there is a region of "anomolously" low magnetic field strength in the south Atlantic. The effect is that many trapped particles whose mirror points would normally be above the atmosphere will here enter the atmosphere and be lost. The south Atlantic anomoly may have an effect as

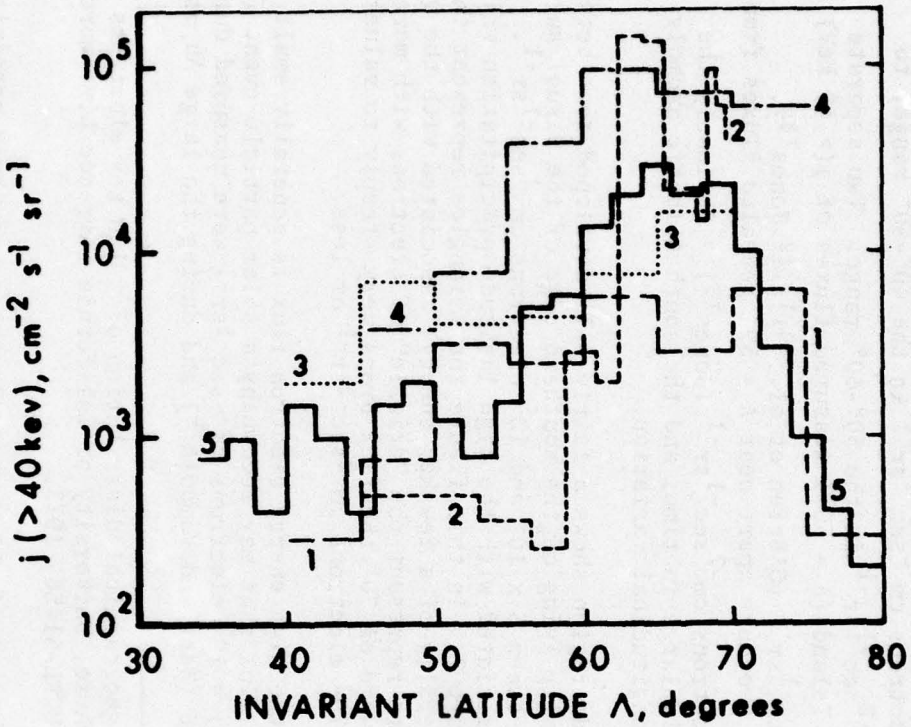

Figure 6. Average intensities at $\lesssim$ 1100 km altitude of precipitated electrons $\geqslant$ 40 keV, observed by the following satellites. (1) Injun 1 during June-September 1961 [O'Brien, 1962], (2) Injun 3, January 1963 [O'Brien, 1964], (3) Injun 3, February-October 1963 [Fritz, 1967, 1968], (4) Explorer 12, August-September 1961 [O'Brien and Laughlin, 1963], (5) Alouette, October 1962 to January 1963 [McDiarmid et al., 1963]. From Potemra and Zmuda (1970).

high as $\Lambda = 50°$ in that region; also there appears to be a diffuse belt of enhanced radiation between $\Lambda = 20° - 40°$ across the north Pacific (Seward[9]).

Precipitating electron fluxes in the midlatitudes vary from $j(> 40 \text{ keV}) \simeq 10^3$ electrons $cm^{-2}sec^{-1}sr^{-1}$ in the 40°-50° range, to 10^3-10^4 electrons $cm^{-2}sec^{-1}sr^{-1}$ in the 50°-60° range. Two separate flights from Wallops Island ($\Lambda = 50°$) measured fluxes of $j(> 40 \text{ keV}) =$ 7-10 electrons $cm^{-2}sec^{-1}sr^{-1}$ (O'Brien et al.;[10,11,12] Jones[13]). Likewise two flights two days apart near $\Lambda = 59°$ revealed fluxes from $2 \times 10^2 - 2 \times 10^4$ electrons $cm^{-2}sec^{-1}sr^{-1}$ (Jones[13]). Obviously the variation is extremely large in time, and the south Atlantic anomoly undoubtedly adds a longitudinal variation.

The high latitude region shows a fairly well developed zone between $\Lambda = 60° - 70°$, generally lying on the southern edge of the visual auroral zone. Fluxes fall between 5×10^3 and 10^5 electrons $cm^{-2}sec^{-1}sr^{-1}$. There is a time pattern associated with the high latitude precipitation which is summarized in Figure 7. In this figure the triangles represent the discrete fluxes (generally of a few keV energy) associated with the visual aurora, while the dots represent the "drizzle" of electrons with more than 40 keV energy. Poleward of 70° the flux drops very steeply to values on the order of 2×10^2 electrons $cm^{-2}sec^{-1}sr^{-1}$ or less.

Over the poles the high energy electron flux is generally small with the exception of the flux that may accompany a solar particle event (SPE). Fluxes of $j(> 40 \text{ keV}) \simeq 10^5$ electrons $cm^{-2}sec^{-1}sr^{-1}$ were measured during the November 1969 SPE (West and Vampola[14]) and during the large August 1972

---

[9] Seward, F.D., The geographical distribution of ~ 100 keV electrons above the earth's atmosphere, University of California Lawrence Livermore Laboratory Report UCRL-51456, 1973.

[10] O'Brien, B.J., Lifetimes of outer-zone electrons and their precipitation into the atmosphere, J. Geophys. Res., 67(10), 3687-3706, 1962.

[11] O'Brien, B.J., High-latitude geophysical studies with satellite Injun 3.3; Precipitation of electrons into the atmosphere, J. Geophys. Res., 69(1), 13-43, 1964.

[12] O'Brien, B.J. and C.D. Laughlin, Electron precipitation and the outer radiation zone, Space Res., 3, 399-417, 1963.

[13] Jones, W.H., COSPAR symposium of D- and E-region ion chemistry, Aeronomy Report No. 48, Univ. of Illinois, Urbana, IL, 1972.

[14] West, Jr., H.I. and A.L. Vampola, Simultaneous observations of solar flare electron spectra in interplanetary space and within the earth's magnetosphere, Phys. Rev. Letters, 26, 458-462, 1971.

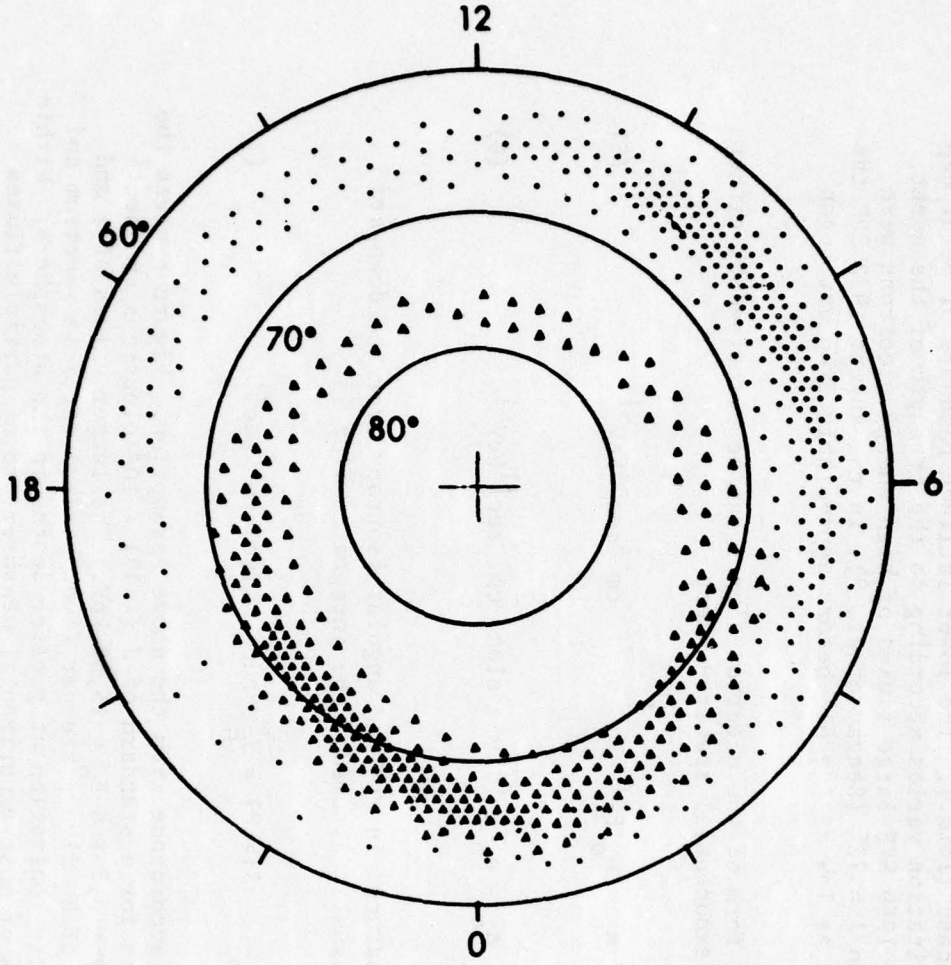

Figure 7. An idealized representation of the two main zones of auroral particle precipitation in the northern hemisphere, where the average intensity of the influx is indicated very approximately by the density of symbols and the coordinates are geomagnetic latitude and geomagnetic time. The discrete events and the associated splash type precipitation are represented by the triangles, and the diffuse events together with the drizzle type of precipitation are indicated by the dots. From Hartz and Brice (1967).

SPE fluxes on the order of 7×10^5 electrons $cm^{-2}sec^{-1}sr^{-1}$ were found (Reagan[15]). These electron fluxes are apparently accompanied by a proton flux although the converse is not true. Electrons may account for up to 40% of the particle-produced ionization in the region of the mesopause, but the proportion drops to essentially zero as the stratopause is approached (*Ibid.*). The lower latitude boundary of polar cap particle precipitation varies according to the strength of the event. In the November 1969 SPE large fluxes of high energy electrons were measured down to $\Lambda = 72°$ (Reagan et al.[16]); in the August 1972 SPE the fluxes extended as low as $\Lambda = 61°$ before appreciable drop off began (Reagan[15]).

The actual form of the electron fluxes can be described by either a power law or exponential spectrum where

$$n_e = n_o E^{-\gamma} \quad \text{elec. } cm^{-2}sec^{-1}keV^{-1} \tag{5}$$

or

$$n_e = n_o e^{-E/E_o} \quad \text{elec. } cm^{-2}sec^{-1}keV^{-1} \; . \tag{6}$$

E and E_o are measured in keV and angular isotropy over the downward hemisphere is usually assumed. The integrated flux is

$$J(> E) = \int_E^\infty ndE \quad \text{elec. } cm^{-2}sec^{-1} \tag{7}$$

and $J = 2\pi j$ in accordance with the above assumption. Figure 8 gives the different fluxes for a standard of $J\ (> 40) = 10^3$ electrons $cm^{-2}sec^{-1}$ and values of $\gamma = 3,5$ and $E_o = 15,50$ keV. The larger values of γ and smaller values of E_o give a steeper (i.e. harder) particle spectrum and consequently less ionization at greater depths in the atmosphere. Within the constraints of most experimental measurements of particle fluxes either the power law or exponential form may be used.

---

[15] Reagan, J.B., A study of the D-region ionosphere during the intense solar particle events of August 1972, Space Sciences Laboratory, Lockheed Palo Alto Research Laboratory, LMSC/D54290, 94 pp, 1975.

[16] Reagan, J.B., W.L. Imhof and E.E. Gaines, Satellite measurements of energetic solar protons, alpha particles, electrons and auroral particles during the 2 November 1969 PCA event, Proceedings of COSPAR symposium on solar particle event of November 1969, J.C. Ulwick (ed.), AFCRL Special Reports, No. 144, 141-166, 1972.

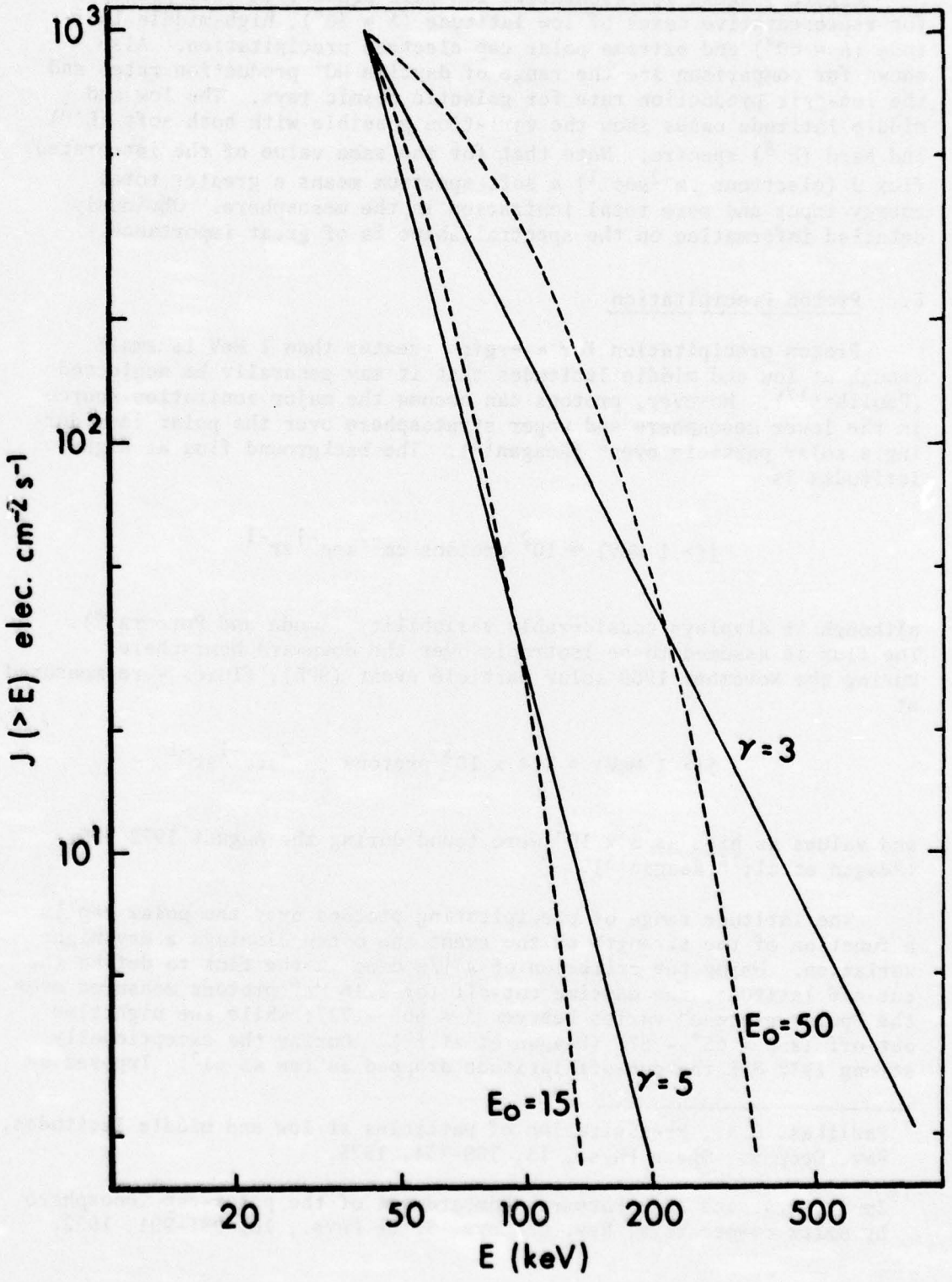

Figure 8. The (integrated) spectra for electron precipitation illustrating two cases each for power law and exponential spectra. The number of electrons > 40 keV has been set equal to 10^3 cm^{-2}s^{-1} in each case.

Figure 9 shows representative ion-pair production rate profiles for representative cases of low latitude ($\Lambda = 30°$), high-middle latitude ($\Lambda = 60°$) and extreme polar cap electron precipitation. Also shown for comparison are the range of daytime NO^+ production rates and the ion-pair production rate for galactic cosmic rays. The low and middle latitude cases show the variation possible with both soft (E^{-3}) and hard (E^{-5}) spectra. Note that for the same value of the integrated flux J (electrons $cm^{-2}sec^{-1}$) a soft spectrum means a greater total energy input and more total ionization in the mesosphere. Obviously detailed information on the spectral shape is of great importance.

E. Proton Precipitation

Proton precipitation for energies greater than 1 MeV is small enough at low and middle latitudes that it may generally be neglected (Paulikas[17]). However, protons can become the major ionization source in the lower mesosphere and upper stratosphere over the polar caps during a solar particle event (Reagan[15]). The background flux at high latitudes is

$$j(> 1 \text{ MeV}) \approx 10^2 \text{ protons } cm^{-2}sec^{-1}sr^{-1}$$

although it displays considerable variability (Zmuda and Potemra[18]). The flux is assumed to be isotropic over the downward hemisphere. During the November 1969 solar particle event (SPE), fluxes were measured at

$$j(> 1 \text{ MeV}) \simeq 1.4 \times 10^3 \text{ protons } cm^{-2}sec^{-1}sr^{-1}$$

and values as high as 3×10^4 were found during the August 1972 SPE (Reagan et al;[16] Reagan[15]).

The latitude range of precipitating protons over the polar cap is a function of the strength of the event and often displays a day-night variation. Using the criterion of a 1/e drop in the flux to define the cut-off latitude, the daytime cut-off for 2.16 MeV protons measured over the "polar plateau" varies between $\Lambda = 66° - 72°$; while the nighttime cut-off is $\Lambda = 65° - 67°$ (Reagan et al.[16]). During the exceptionally strong 1972 SPE the cut-off latitude dropped as low as 61°. Imposed on

---

[17] Paulikas, G.A., Precipitation of particles at low and middle latitudes, Rev. Geophys. Space Phys., 13, 709-734, 1975.

[18] Zmuda, A.J. and T.A. Potemra, Bombardment of the polar-cap ionosphere by solar cosmic rays, Rev. Geophys. Space Phys., 10, 981-991, 1972.

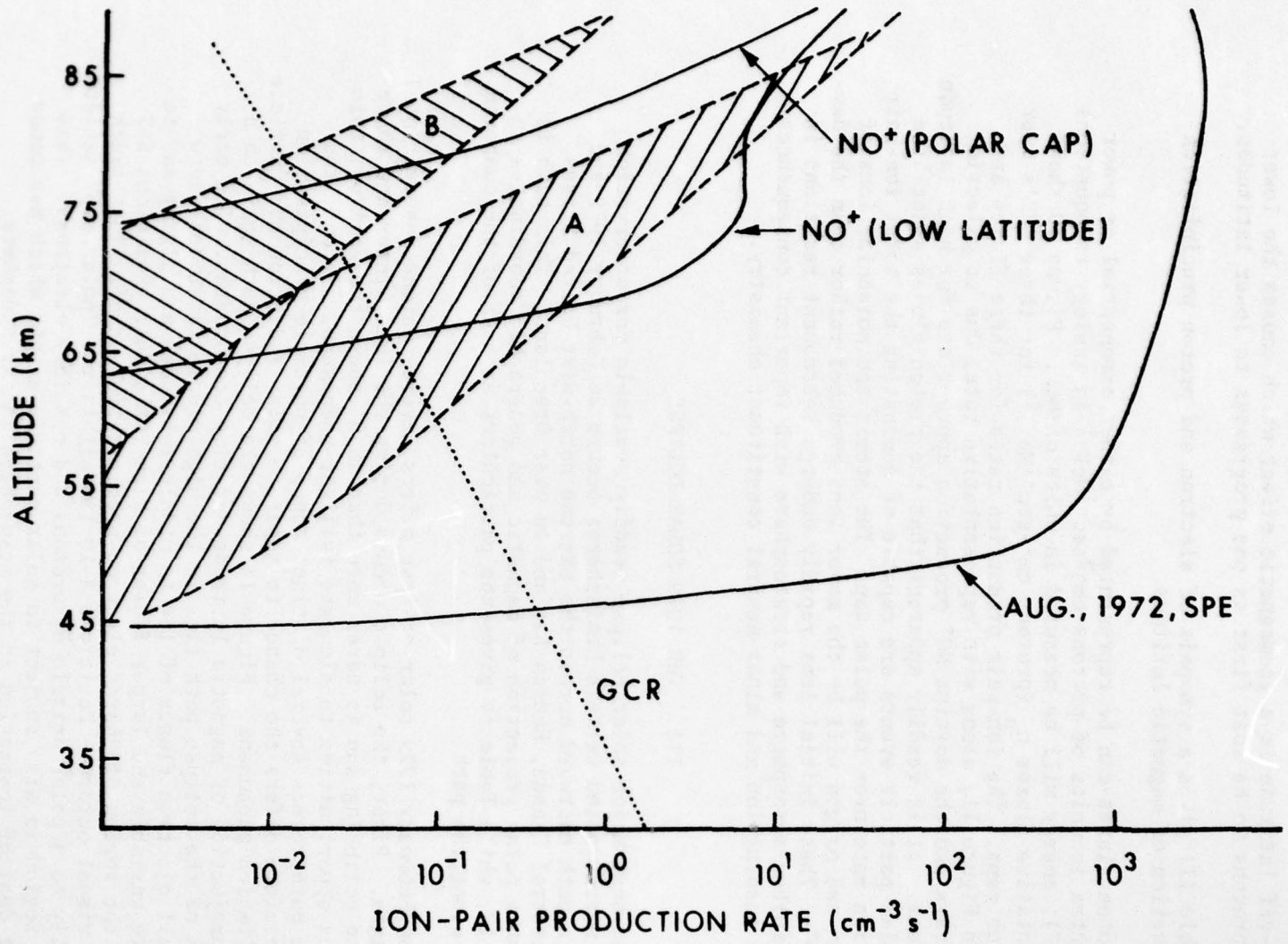

Figure 9. The ion-pair production rate profiles for representative high latitude (A) and low latitude (B) electron spectra. For each case the variation due to a hard spectrum (γ = 5) and soft spectrum (γ = 3) is shown by the cross-hatching. Also shown are two solar radiation ion-pair production rate profiles and the profile from galactic cosmic rays and the August 1972, solar particle event (electron precipitation).

the cut-off latitude is a geomagnetic effect which causes the lower energy protons to be lost first as one progresses to lower latitudes.

Table III gives a synopsis of electron and proton precipitation as a function of magnetic latitude.

Proton fluxes can be represented by either exponential or power law spectra in units of protons $cm^{-2}sec^{-1}MeV^{-1}$ in analogy to equations (5) - (7); energy will be measured in units of MeV. Figure 10 shows representative fluxes n_p (protons $cm^{-2}sec^{-1}MeV^{-1}$) for three SPE's over the polar caps. The ion-pair production rates for these fluxes are shown in Figure 11, along with representative rates due to galactic cosmic rays and the daytime NO^+ production appropriate for high latitude conditions. It is readily apparent that the proton fluxes associated with solar particle events are capable of dominating the total ion-pair production rate over the polar cap. The atomic and molecular ions of nitrogen and oxygen will be the major ions produced rather than the daytime NO^+. These initial ions rapidly undergo subsequent reactions in the disturbed mesosphere and stratosphere with important consequences for the ensuing ion and minor-neutral constituent chemistry.

III. THE 1979 SOLAR ECLIPSE

The next major solar eclipse readily available for observation in the northern and western hemispheres occurs 26 February 1979 and traces a path eastward across the extreme north-west United States, south-central Canada, Hudson Bay and on over Greenland. This path is shown on a polar projection of magnetic and geographic coordinates in Figure 12, while Table IV gives the particulars at each of the numbered points along the path.

The February 1979 solar eclipse offers several unique observational advantages. First, the eclipse occurs during the late winter and therefore the eclipsing sun is never more than 25.5° above the horizon; this provides opportunities to simulate twilight phenomena. Second, the eclipse path covers several distinct zones of particle precipitation and therefore offers the chance to separate solar radiation and particle precipitation phenomena. Figure 13 shows the eclipse path again on a polar projection of magnetic latitude and time coordinates. The early portion of the eclipse path lies in the high-middle latitudes where the small electron fluxes of low to middle latitudes are giving way to the more variable and larger fluxes of high latitudes. Positions 5-7 lie in the region of "hard" electron precipitation usually just south of the visual aurora. Positions 8-10 lie within the "polar cap" subject generally to a polar drizzle of protons and possibly electrons. This latter region is also subject to solar particle events which may cause a great deal of ionization in the mesosphere and stratosphere.

TABLE III

Magnetic Latitude	Electron Flux (> 40 keV) ($cm^{-2}sec^{-1}sr^{-1}$)	Proton Flux (> 1 MeV) ($cm^{-2}sec^{-1}sr^{-1}$)
<25°	$<2 \times 10^1$	very small
25°-40°	$\leq 2 \times 10^2$	very small
40°-50°	$\approx 10^3$ (10^1 - 10^4)	very small
50°-60°	$\approx 3 \times 10^3$ (10^1 - 10^5)	small
60°-70°	$\approx 10^4$ (2×10^3 - 2×10^5)	small
70°-75°	$10^5 \rightarrow 2 \times 10^2$	small
>75°	$<10^2$	$\approx 10^2$ (5 - 5×10^2)
Solar Particle Event	up to 5×10^5	up to 3×10^4

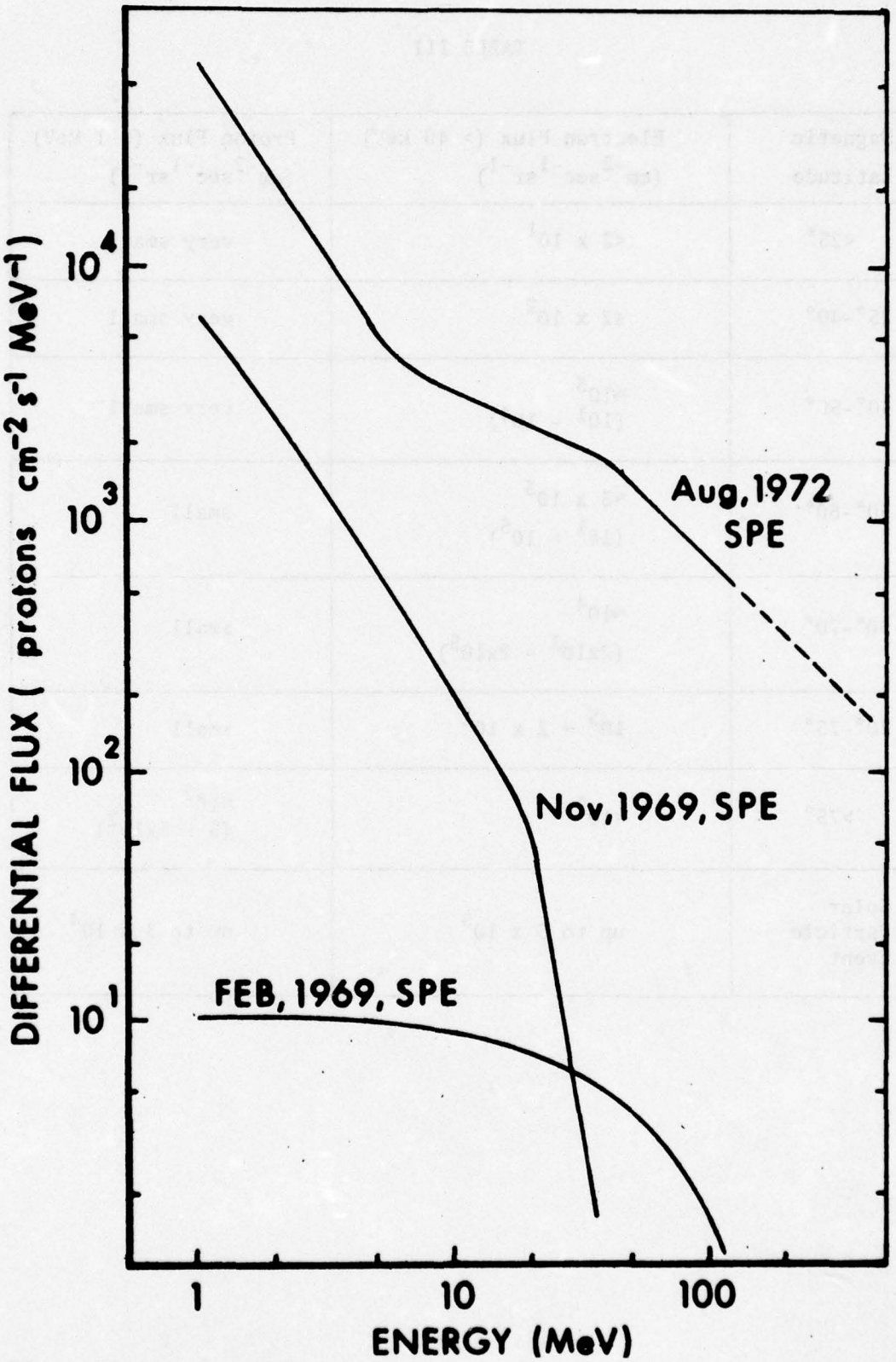

Figure 10. Differential proton fluxes for selected solar particle events.

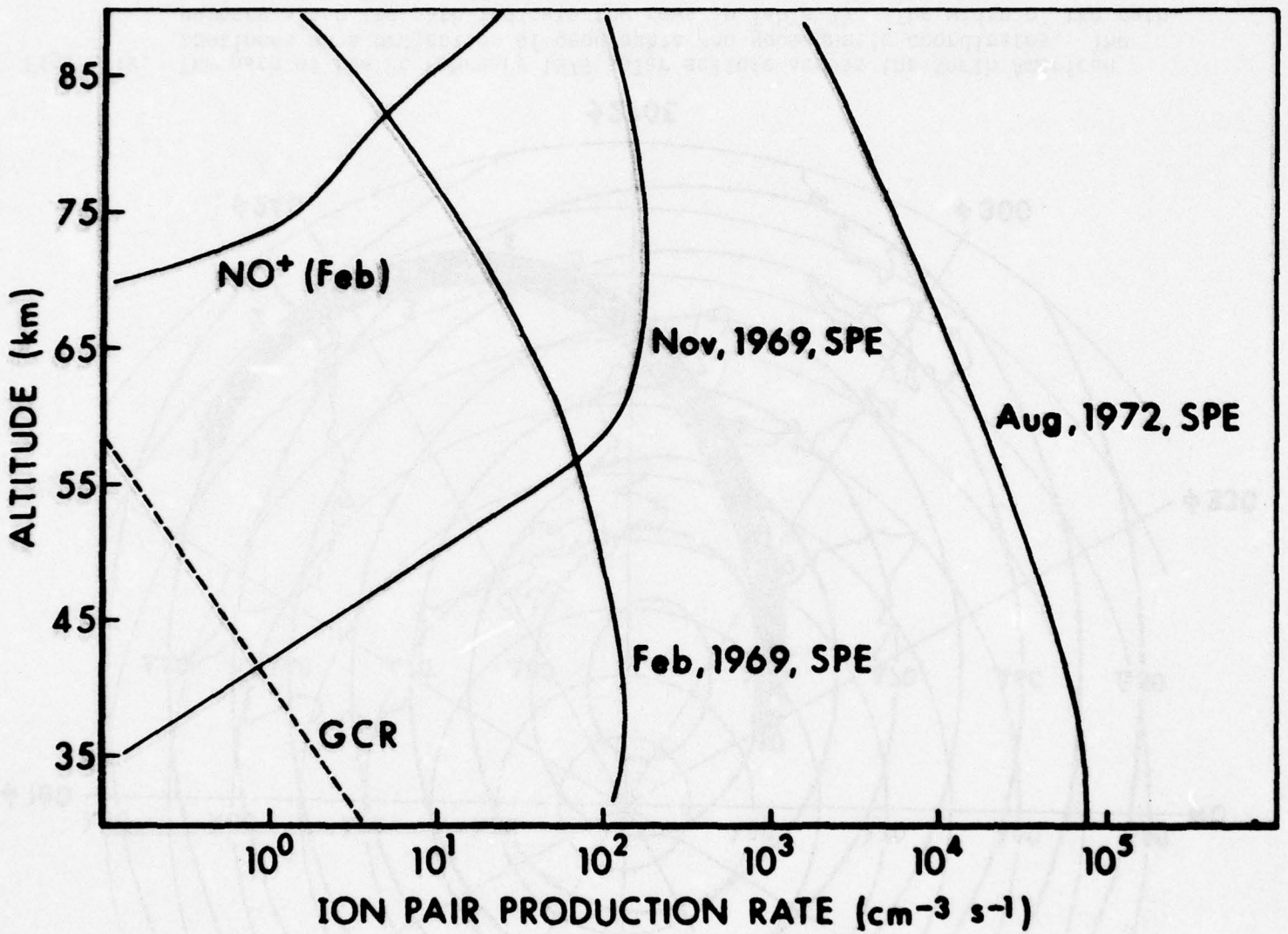

Figure 11. The ion-pair production rates due to protons for selected solar particle events shown in Figure 10. Also shown for comparison are the ion-pair production rates for galactic cosmic rays and the NO^+ production rate from the solar flux appropriate for high latitudes.

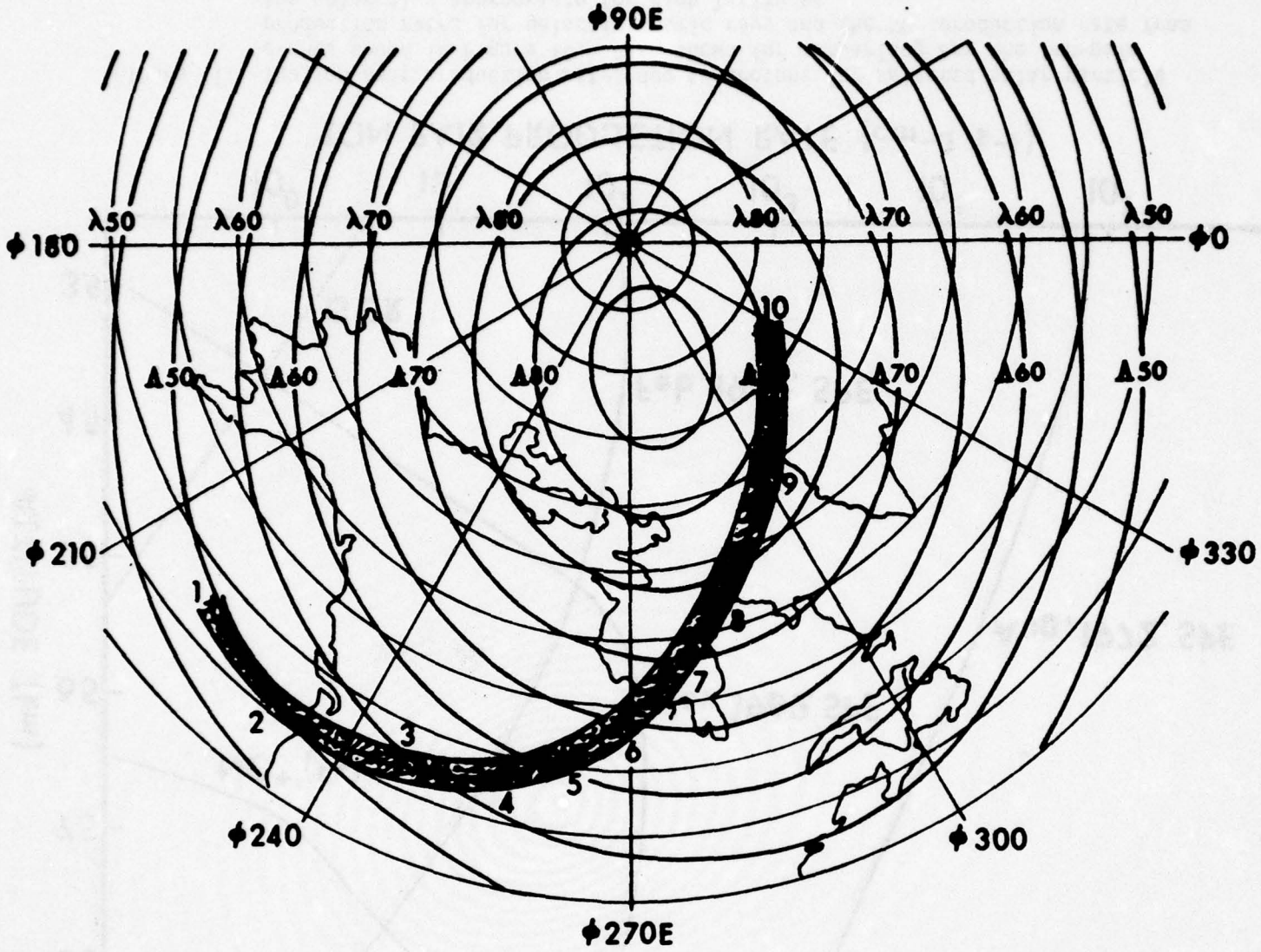

Figure 12. The path of the 26 February 1979 solar eclipse across the North American continent on a projection of geographic and geomagnetic coordinates. The numbers along the path indicate the rows in Table IV. The width of the path approximately indicates the area where totality may be observed.

TABLE IV

	GEOGRAPHIC LONG.	GEOGRAPHIC LAT.	MAGNETIC LONG.	MAGNETIC LAT.	EPHEMERIS TIME+	GEOGRAPHIC LOCAL TIME*	MAGNETIC LOCAL TIME	SUN ANGLE	ECLIPSE DURATION	SHADOW WIDTH
					h m	h m	h m		m s	km
1	139.38°W (220.62)	47.28°	282°	49°	16:09.9	07:09.9	05:37	0.0°	1 49	227
2	129.04 (230.96)	46.08	293°	50	16:12	07:12	06:24	7.5	2 05	253
3	113.87 (246.13)	46.40	309°	54	16:24	09:24	07:40	18.4	2 30	295
4	105.30 (254.70)	48.10	321°	58	16:36	09:36	08:40	23.2	2 43	307
5	98.29 (261.37)	50.46	330°	61½	16:48	10:48	09:28	25.4	2 48	304
6	91.63 (268.37)	53.42	337°	65	17:00	11:00	10:08	25.5	2 48	292
7	84.46 (275.54)	57.11	345°	68½	17:12	12:12	10:52	23.6	2 43	277
8	75.40 (284.60)	61.96	3	73½	17:24	12:24	12:16	19.3	2 32	259
9	58.71 (301.29)	69.78	40	78	17:36	13:36**	14.56	10.0	2 09	240
10	33.99 (326.01)	77.18	87	80½	17:39.2	15:39.2	15:11	0.0	1 42	227

\+ subtract approximately 0.65 minutes to obtain universal time
* assumes standard time (Rand-McNally World Atlas, 1967 ed)
** referred to Greenland

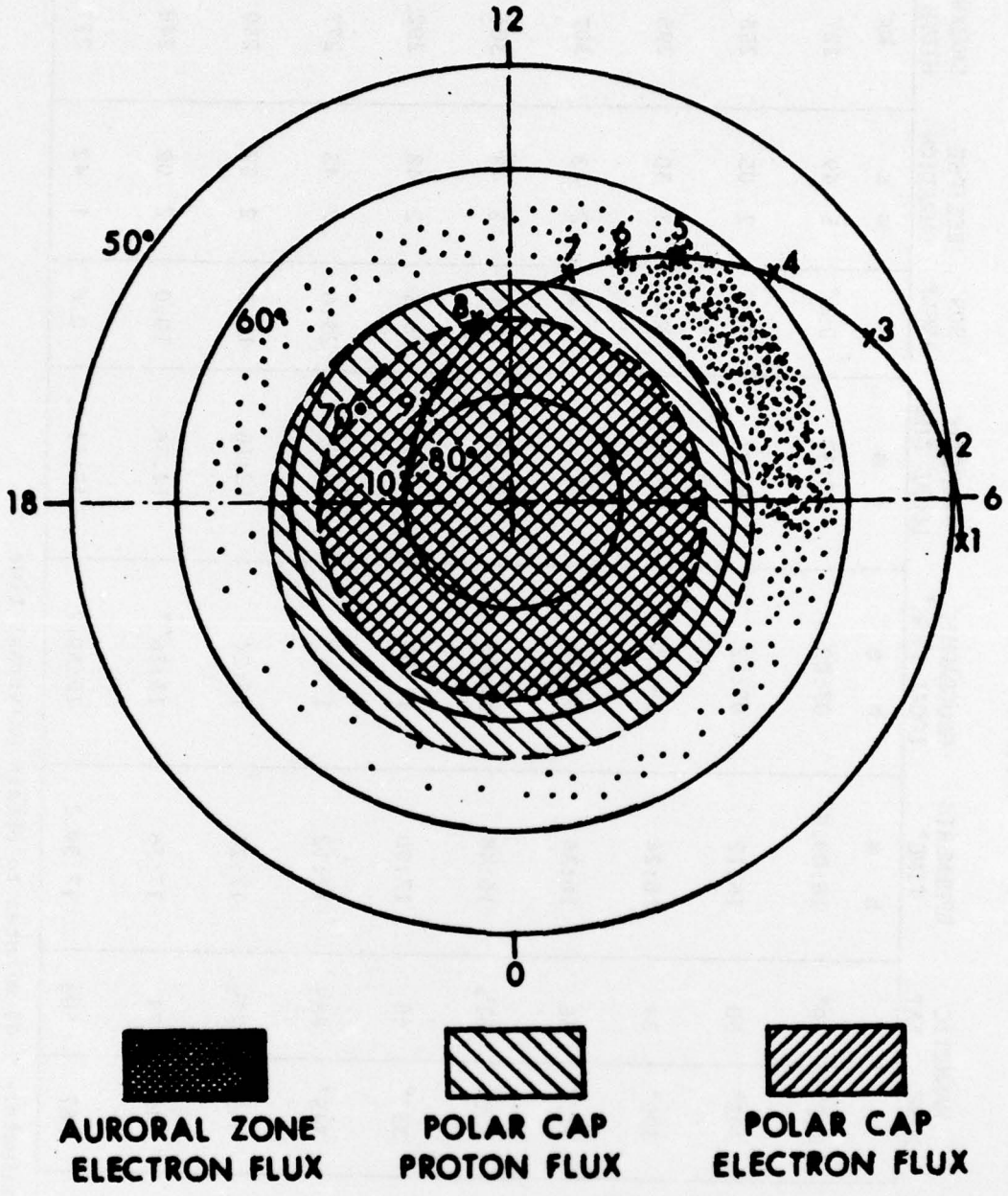

Figure 13. The 26 Feb 79 solar eclipse path as it intersects various zones of particle precipitation; projected on magnetic coordinates.

The probable levels of ion-pair production along the eclipse path will next be illustrated and suggestions will be offered as to specific experimental measurements which should be attempted. Figure 14 gives the components of the ion-pair production rate near Yakima, Washington, midway between positions 2 and 3:

solar zenith angle = 72.5°

j_e (> 40 keV) = 3×10^3 elec. $cm^{-2}sec^{-1}sr^{-1}$

j_p (> 1 MeV) = 0. (10^1 - 10^5 is range of fluxes)

In the non-eclipse situation the NO^+ production would be of the same order of magnitude as the potential ion-pair production rate due to particle precipitation throughout the upper mesosphere. Galactic cosmic rays will be the dominant source of ionization in the stratosphere. The biggest variable is the particle precipitation, both its magnitude and spectral shape. The absence of a direct source of NO^+ during the eclipse will alter the ion chemistry and the general lack of sunlight will greatly alter the negative ion chemistry.

Figure 15 shows the possible ion-pair production rates at position 5, located approximately 100 km north of Winnipeg, Manitoba, Canada:

solar zenith angle = 62.7°

j_e (> 40 keV) = 2×10^4 elec. $cm^{-2}sec^{-1}sr^{-1}$

j_p (> 1 MeV) = 0. (10^1 - 10^5 is range of fluxes)

Electron precipitation could likely be the dominant ion source throughout the mesosphere. Of particular interest is the absence of sunlight on the negative ion chemistry in the presence of another large source of ionization.

Figure 16 shows the situation at position 8, located near the Hudson Straits. For "polar drizzle", the most likely case, one has

j_e (> 40 keV) < 10^2 electrons $cm^{-2}sec^{-1}sr^{-1}$

j_p (1 MeV) $\approx 10^2$ protons $cm^{-2}sec^{-1}sr^{-1}$

solar zenith angle = 71.6°

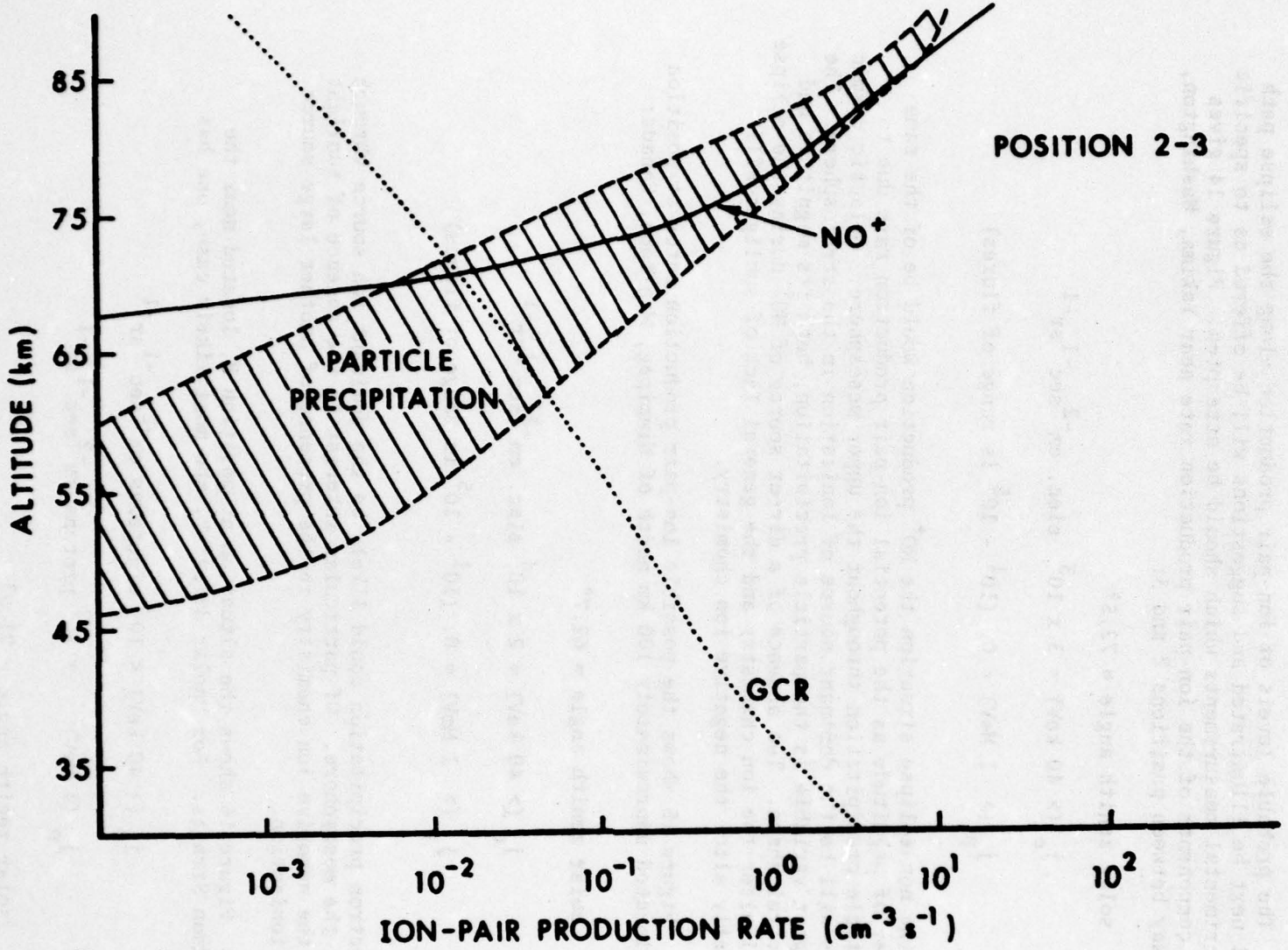

Figure 14. The ion-pair production rate profiles for various sources at points between positions 2 and 3 along the solar eclipse path. Variation in particle precipitation profiles is for hard and soft differential electron fluxes for a set of total flux of j (> 40 keV) = 2×10^4 electrons $cm^{-2} sec^{-1} sr^{-1}$.

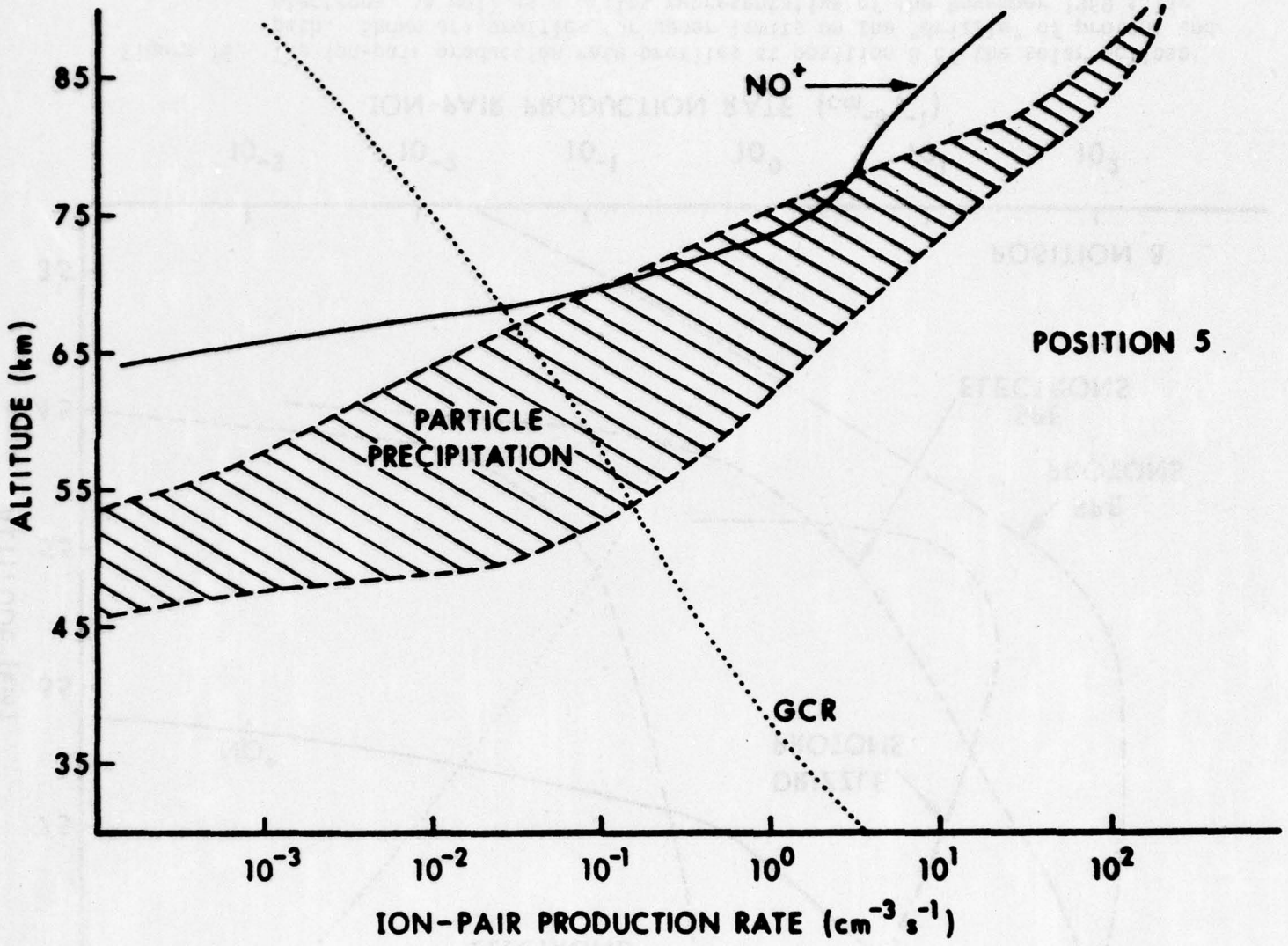

Figure 15. The ion-pair production rate profiles at position 5 of the solar eclipse path. Variation in particle precipitation profiles is for hard and soft differential electron fluxes for a set total flux of j (> 40 keV) = 2×10^4 electrons $cm^{-2} sec^{-1} sr^{-1}$.

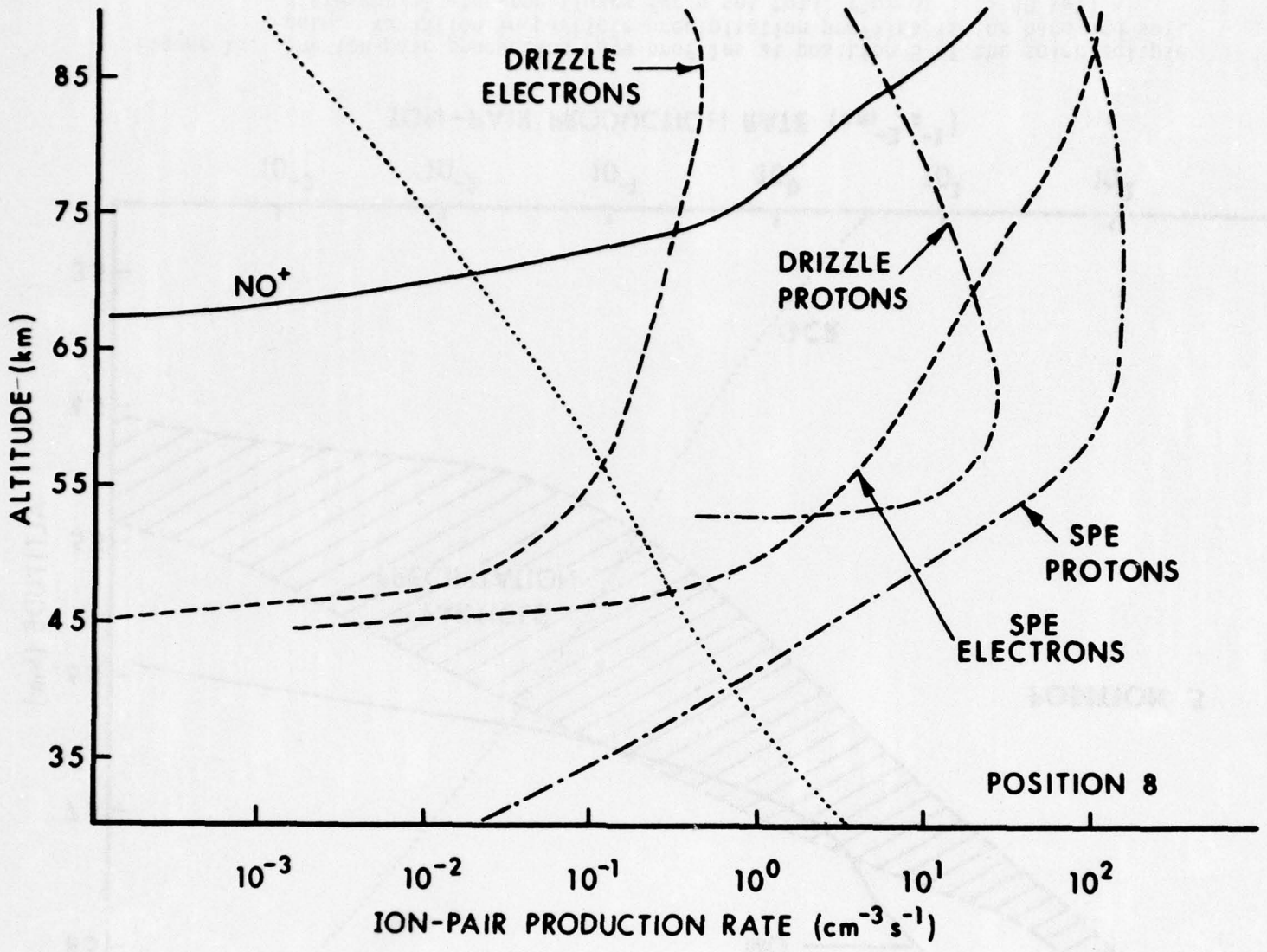

Figure 16. The ion-pair production rate profiles at position 8 of the solar eclipse path. Shown are profiles for upper limits on the "drizzle" of protons and electrons, as well as profiles representative of the November 1969 solar particle event. The dotted line represents GCR production rate.

The polar drizzle may be the larger source of ionization at the more northern positions along the eclipse path, and it is crucial to get an accurate measurement of the energy spectrum of such particles.

There is also the possibility that a solar particle event will be in progress at the time of the eclipse and completely dominate the ion production mechanism. The ion-pair production rate profiles for the November 1969 solar particle event are also shown in Figure 16 where

$$j_e = 2.4 \times 10^4 \text{ electrons cm}^{-2}\text{sec}^{-1}\text{sr}^{-1}$$

$$j_p = 1.4 \times 10^3 \text{ protons cm}^{-2}\text{sec}^{-1}\text{sr}^{-1}$$

and the differential flux is proportional to $E^{-2.94}$ for the electrons (40 keV - 3 MeV) and the same as that shown for the protons in Figure 10 for the August 1972 SPE. Previous measurements under such conditions indicate a simplified ion chemistry.

In order to accurately define the ion chemistry of the mesosphere and stratosphere, the neutral [NO] profile should be carefully monitored, since this is critical for the NO^+ ion-pair production rate. Because particle precipitation is such a variable quantity, "in-situ" measurements during the solar eclipse are necessary. Care should be taken when satellite measurements are used to insure they are on the same magnetic field line as the ground observation site. In addition, the energy spectrum of particle precipitation should be determined since this is as crucial to the ionization profile as the total flux. Particular attention should be directed to the energy dependence of protons of more than 10 MeV energy and relativistic electrons.

IV. SUMMARY

The ion chemistry of the stratosphere and mesosphere depends on the type of initial or precursor ions produced and, of course, their magnitude of production. In the daytime upper mesosphere NO^+ is the predominant initial ion. In the stratosphere and lower mesosphere the predominant initial ion is O_2^+. Precipitation of energetic particles can produce an O_2^+ - initiated ion chemistry throughout the entire mesosphere, and greatly enhance production at all altitudes.

A solar eclipse offers unique opportunities to ascertain the balance between an O_2^+ and NO^+ dominated ion chemistry. Care should be taken to provide coordinated measurements of the neutral [NO] profile as well as the flux and energy spectra of precipitating particles.

REFERENCES

1. Swider, W., Jr., Ionization rates due to the attenuation of 1-100Å nonflare solar x-rays in the terrestrial atmosphere, Rev. Geophysics, 7, 573-594, 1969.

2. Banks, P.M. and G. Kockarts, Aeronomy, Part A, Academic Press, New York, 1973.

3. Nicolet, M. and A.C. Aikin, The formation of the D region of the ionosphere, J. Geophys. Res., 65, 1469-1483, 1960.

4. Meira, L.G., Rocket measurements of upper atmospheric nitric oxide and their consequences to the lower ionosphere, J. Geophys. Res., 76, 202-212, 1971.

5. Heaps, M.G., The ion-pair production rate due to cosmic rays, BRL Memorandum Report No. 2641, 1976.

6. Karszenbaum, H. and D.A. Gagliardini, Galactic x-ray sources and the ionosphere D region, Nature, 257, 34-35, 1975.

7. Rapp, D., P. Englander-Golden and D.D. Briglia, Cross sections for dissociative ionization of molecules by electron impact, J. Chem. Phys., 42, 4081-4086, 1965.

8. Winters, H.F., Ionic absorption and dissociation cross section for nitrogen, J. Chem. Phys., 44, 4472-4476, 1966.

9. Seward, F.D., The geographical distribution of ~100 keV electrons above the earth's atmosphere, University of California, Lawrence Livermore Laboratory Report UCRL-51456, 1973.

10. O'Brien, B.J., Lifetimes of outer-zone electrons and their precipitation into the atmosphere, J. Geophys. Res., 67(10), 3687-3706, 1962.

11. O'Brien, B.J., High-latitude geophysical studies with satellite Injun 3.3; Precipitation of electrons into the atmosphere, J. Geophys. Res., 69(1), 13-43, 1964.

12. O'Brien, B.J., and C.D. Laughlin, Electron precipitation and the outer radiation zone, Space Res., 3, 399-417, 1963.

13. Jones, W.H., COSPAR symposium of D- and E-region ion chemistry, Aeronomy Report No. 48, Univ. of Illinois, Urbana, IL, 1972.

14. West,Jr., H.I., and A.L. Vampola, Simultaneous observations of solar flare electron spectra in interplanetary space and within the earth's magnetosphere, Phys. Rev. Letters, 26, 458-462, 1971.

15. Reagan, J.B., A study of the D-region ionosphere during the intense solar particle events of August 1972, Space Sciences Laboratory, Lockheed Palo Alto Research Laboratory, LMSC/D454290, 94 pp, 1975.

16. Reagan, J.B., W.L. Imhof and E.E. Gaines, Satellite measurements of energetic solar protons, alpha particles, electrons and auroral particles during the 2 November 1969 PCA event, Proceedings of COSPAR symposium on solar particle event of November 1969, J.C. Ulwick (ed.), AFCRL Special Reports No. 144, 141-166, 1972.

17. Paulikas, G.A., Precipitation of particles at low and middle latitudes, Rev. Geophys. Space Phys., 13, 709-734, 1975.

18. Zmuda, A.J. and T.A. Potemra, Bombardment of the polar-cap ionosphere by solar cosmic rays, Rev. Geophys. Space Phys., 10, 981-991, 1972.

BIBLIOGRAPHY

Brasseur, G. and M. Nicolet, Chemospheric processes of nitric oxide in the mesosphere and stratosphere, Planet. Space Sci., 21, 939-961, 1973.

Fritz, T.A., Spectral, spatial, and temporal variations observed for outer zone electrons from 10 to 100 keV with satellite Injun 3, Ph.D. thesis, University of Iowa, Iowa City, 1967.

Fritz, T.A., High-latitude outer zone boundary region for $\geq$ 40-keV electrons during geomagnetically quiet periods, J. Geophys. Res., 72(23), 7245-7255, 1968.

Hartz, T.R. and N.M. Brice, The general pattern of auroral particle precipitation, Planet Space Sci., 15, 301-329, 1967.

Heroux, L., M. Cohen, and J.E. Higgins, Electron densities between 110 and 300 km derived from solar EUV fluxes of August 23, 1972, J. Geophys. Res., 79, 5237-5244, 1974.

Manson, J.E., The spectrum of the quiet sun between 30Å and 128Å for November 1965, Astrophys. J., 147, 703-710, 1967.

McDiarmid, I.B., J.R. Burrows, E.E. Budzinski, and M.D. Wilson, Some average properties of the outer radiation zone at 1000 km, Can. J. Phys., 41, 2064-2079, 1963.

Meeus, J., C.C. Grossjean and W. Vanderleen, Cannon of Solar Eclipses, Pergamon Press, 749 pp., 1966.

Potemra, T.A. and A.J. Zmuda, Precipitating energetic electrons as an ionization source in the midlatitude nighttime D region, J. Geophys. Res., 75, 7161-7167, 1970.

DISTRIBUTION LIST

No. of Copies	Organization
12	Commander Defense Documentation Center ATTN: DDC-TCA Cameron Station Alexandria, VA 22314
1	Director Institute for Defense Analyses ATTN: Dr. E. Bauer 400 Army-Navy Drive Arlington, VA 22202
2	Director Defense Advanced Research Projects Agency ATTN: STO, CPT J. Justice, LTC W. A. Whitaker 1400 Wilson Boulevard Arlington, VA 22209
2	Director of Defense Research and Engineering ATTN: Mr. D. Brockway CAPT K. Ruggles Washington, DC 20305
4	Director Defense Nuclear Agency ATTN: STAP (APTL) STRA (RAAE) Dr. C. Blank Dr. H. Fitz, Jr. DDST Washington, DC 20305
2	DASIAC/DOD Nuclear Information and Analysis Center General Electric Company-TEMPO ATTN: Mr. A. Feryok Mr. W. Knapp 816 State Street P.O. Drawer QQ Santa Barbara, CA 93102
1	Director Defense Communications Agency ATTN: Code 340, Mr. W. Dix Washington, DC 20305
1	Commander US Army Materiel Development and Readiness Command ATTN: DRCDMA-ST 5001 Eisenhower Avenue Alexandria, VA 22333
1	Commander US Army Aviation Research and Development Command ATTN: DRSAV-E 12th and Spruce Streets St. Louis, MO 63166
1	Director US Army Air Mobility Research and Development Laboratory Ames Research Center Moffett Field, CA 94035
1	Commander US Army Electronics Command ATTN: DRSEL-RD Fort Monmouth, NJ 07703
4	Commander/Director US Army Electronics Command Atmospheric Sciences Laboratory ATTN: Dr. E. H. Holt Mr. N. Beyers Mr. F. Horning Dr. F. E. Niles White Sands Missile Range, NM 88002
1	Commander US Army Missile Command ATTN: DRSMI-R Redstone Arsenal, AL 35809

DISTRIBUTION LIST

No. of Copies	Organization
1	Commander US Army Tank Automotive Development Command ATTN: DRDTA-RWL Warren, MI 48090
1	Commander US Army Mobility Equipment Research & Development Command ATTN: Tech Docu Cen, Bldg. 315 DRSME-RZT Fort Belvoir, VA 22060
1	Commander US Army Armament Command Rock Island, IL 61202
1	Commander, USACEEIA ATTN: CCC-CED-EMED (Miles Merkel) Fort Huachuca, AZ 85635
2	Commander US Army Harry Diamond Labs ATTN: DRXDO-TI DRXDO-NP, Mr. F. Wimenitz 2800 Powder Mill Road Adelphi, MD 20783
1	Director US Army TRADOC Systems Analysis Agency ATTN: ATAA-SA White Sands Missile Range NM 88002
1	Commander US Army Nuclear Agency ATTN: Dr. J. Berberet Fort Bliss, TX 79916
3	Commander US Army Research Office ATTN: Dr. A. Dodd, Dr. D. Squire Dr. R. Lontz P.O. Box 12211 Research Triangle Park, NC 27709
2	Director US Army BMD Advanced Technology Center ATTN: Mr. M. Capps Mr. W. Davies P.O. Box 1500 Huntsville, AL 38507
2	Commander US Army BMD System Command ATTN: SSC-HS, Mr. H. Porter SSC-TET, Mr. E. Carr P.O. Box 1500 Huntsville, AL 35807
1	Director US Army Ballistic Missile Defense Technology Office ATTN: M. C. McClain Arlington, VA 22209
1	HQDA (DACS-BMT) Arlington, VA 22209
1	HQDA (DAEN-RDM/Dr. F. de Percin) Washington, DC 20314
3	Commanding Officer US Army Research & Development Group (Europe) ATTN: Dr. H. Lemons, Dr. G. R. Husk, LTC J. Kennedy Box 15 FPO New York 09510
1	Chief of Naval Research ATTN: Code 418, Dr. J. Dardis Department of the Navy Washington, DC 20360
1	Commander US Naval Surface Weapons Center ATTN: Dr. L. Rutland Silver Spring, MD 20910

DISTRIBUTION LIST

No. of Copies	Organization
1	Commander US Naval Surface Weapons Center ATTN: Mr. W. Moler San Diego, CA 92152
4	Commander US Naval Research Laboratory ATTN: Dr. W. Ali Dr. D. Strobel Code 7700, Mr. J. Brown Code 2020, Tech Lib Washington, DC 20375
4	HQ USAF (AFNIN; AFRD; AFRDQ; ARTAC, COL C. Anderson) Washington, DC 20330
9	AFGL (LKB, Dr.K.Champion, Dr. W.Swider, Dr.J.Paulson, Dr. T.Keneshea; LKD, Dr.R.Narcisi; OPI, Dr.J.Garing; OPR, Dr. H. Gardiner, Dr. Murphy, Dr. Kennelly) Hanscom AFB, MA 01730
2	AFSC (DLCAW, LTC R. Linkous; SCS) Andrews AFB Washington,DC 20334
1	Director National Oceanic and Atmospheric Administration US Department of Commerce ATTN: Dr. E. Ferguson Boulder, CO 80302
4	Director Los Alamos Scientific Laboratory ATTN: Dr. Maier (Gp J-10) Dr. J. Zinn (MS 664) Dr. W. Myers Dr. M. Peek P. O. Box 1663 Los Alamos, NM 87544
2	Sandia Laboratories ATTN: Dr. K. J. Touryan Dr. F. Hudson P. O. Box 5800 Albuquerque, NM 87115
4	Director National Aeronautics and Space Administration Goddard Space Flight Center ATTN: Dr. E. Hilsenrath Dr. V. Kunde Dr. A. Aikin Dr. R. Goldberg (Code 912) Greenbelt, MD 20771
2	Director National Science Foundation ATTN: Dr. F. Eden Dr. G. Adams 1800 G. Street, NW Washington, DC 20550
1	Calspan Corporation ATTN: Mr. R. Fluegee P. O. Box 235 Buffalo, NY 14221
2	General Electric Company Valley Forge Space Technology Center ATTN: Dr. M. Bortner Dr. T. Baurer P. O. Box 8555 Philadelphia, PA 19101
1	General Research Corporation ATTN: Dr. J. Ise P. O. Box 3587 Santa Barbara, CA 93105

DISTRIBUTION LIST

No. of Copies	Organization
2	Lockheed Palo Alto Research Laboratory ATTN: Dr. J. Reagan Mr. R. Sears 3251 Hanover Street Palo Alto, CA 94304
1	Mission Research Corporation ATTN: Dr. M. Scheibe 812 Anacapa Street, Studio 5 Santa Barbara, CA 93101
1	Mitre Corporation ATTN: Tech Lib P.O. Box 208 Bedford, MA 01730
1	Pacific-Sierra Research Corporation ATTN: Mr. E. Fields 1456 Cloverfield Blvd. Santa Monica, CA 90404
1	R&D Associates ATTN: Dr. F. Gilmore P.O. Box 9695 Marina Del Rey, CA 90291
1	The Rand Corporation ATTN: Dr. C. Crain 1700 Main Street Santa Monica, CA 90406
2	Science Applications, Inc. ATTN: Mr. R. Lowen, Mr. D. Hamlin 1250 Prospect Plaza La Jolla, CA 90406
1	Science Applications, Inc./ Huntsville ATTN: Mr. R. Byrn 2109 West Clinton Avenue Suite 100 Huntsville, AL 358051
1	Spectra Research Systems, Inc. ATTN: Mr. B. Kilday 2212 Dupont Drive Irvine, CA 92664
1	Stanford Research Institute ATTN: Dr. J. Peterson 333 Ravenswood Avenue Menlo Park, CA 94025
1	Systems Control, Inc. ATTN: Mr. R. Foerster 260 Sheridan Avenue Palo Alto, CA 94306
1	Systems, Science & Software ATTN: Dr. R. Englemore P.O. Box 1620 La Jolla, CA 92037
1	Teledyne-Brown Engineering Company, Inc. SETAC ATTN: D. Lambert Research Park Huntsville, AL 35807
1	TRW Systems Group ATTN: Tech Lib One Space Park Redondo Beach, CA 90278
1	Visidyne, Inc. ATTN: Dr. H. Smith 19 Third Avenue, N.W. Industrial Park Burlington, MA 01803
1	Pennsylvania State University Ionospheric Research Laboratory ATTN: Dr. L. Hale University Park, PA 16802

DISTRIBUTION LIST

No. of Copies	Organization
1	University of Colorado CIRES ATTN: Dr. A. W. Castleman Boulder, CO 80302
2	University of Colorado Joint Institute for Laboratory Astrophysics ATTN: Dr. W. C. Lineberger Dr. A. V. Phelps Boulder, CO 80302
2	University of Denver Denver Research Institute ATTN: Dr. R. Amme Dr. D. Murcray P.O. Box 10127 Denver, CO 80210
1	University of Illinois Dept. of Electrical Engineering ATTN: Dr. C. Sechrist, Jr. Urbana-Champaign Campus Urbana, IL 61801
1	University of Minnesota, Morris Division of Science and Mathematics ATTN: Dr. M. N. Hirsh Morris, MN 56267
2	University of Pittsburgh Cathedral of Learning ATTN: Dr. M. A. Biondi Dr. F. Kaufman 400 Belefield Avenue Pittsburgh, PA 15213
1	University of Texas at El Paso Physics Department ATTN: Ms. J. Collins El Paso, TX 79902
1	Utah State University Center for Research in Aeronomy ATTN: Dr. L. Megill Logan, UT 84321
1	Wayne State University Department of Engineering ATTN: Dr. R. Kummler Detroit, MI 48202
	Aberdeen Proving Ground
	Marine Corps LnO Dir, USAMSAA